Immunogenic cell death in mice expressing caspase-resistant ROCK1 is not replicated by ROCK inhibitors

Gregory Naylor[1,2,3,4], Linda Julian[1,2,4,5], Steven Watson-Bryce[1], Margaret Mullin[6], Robert J Nibbs[7], Michael F Olson[8]

[1]Cancer Research UK Beatson Institute, Garscube Estate, Switchback Road, Glasgow G61 1BD, UK.

[2]Institute of Cancer Sciences, University of Glasgow, Glasgow G12 8QQ, UK.

[3]Present address: Beatson West of Scotland Cancer Centre, NHS Greater Glasgow & Clyde, 1053 Great Western Road, Glasgow, G12 0YN, UK

[4]Equal contribution by these authors

[5]Present address: Cancer Research UK Cambridge Institute, Robinson Way, Cambridge CB2 0RE, UK

[6]Electron Microscopy Facility, School of Life Sciences, University of Glasgow, Glasgow G12 8QQ, UK.

[7]Institute of Infection, Immunity and Inflammation, School of Life Sciences, University of Glasgow, Glasgow G12 8QQ, UK.

[8]Ryerson University, Department of Chemistry and Biology, 661 University Avenue Suite 1105, Toronto ON, M5G 1M1, Canada

Running title: ROCK1 cleavage limits liver immunogenic cell death

Corresponding Author: Professor Michael F Olson, Ryerson MaRS Research Facility, 661 University Avenue Suite 1105, Ryerson University, Toronto ON CANADA, M5G 1M1. Tel: +1 416 979 5000. Email: michael.olson@ryerson.ca

Abstract

The characteristic changes in morphology during apoptosis help facilitate "immunologically-silent" cell death by limiting the release of cellular contents and enabling efficient clearance of apoptotic cell bodies. Caspase-mediated cleavage of the ROCK1 protein kinase results in its constitutive activation, which drives the rapid and forceful contraction of apoptotic cells. We previously showed in Julian *et al*. [1] that when ROCK1 was mutated to render it caspase-resistant, there was greater liver damage and neutrophil recruitment after acute treatment with the hepatotoxin diethylnitrosamine (DEN). We now show that acute DEN-induced liver damage resulted in greater induction of pro-inflammatory cytokines/chemokines, indicative of immunogenic cell death (ICD), in mice expressing non-cleavable ROCK1 (ROCK1nc). Hepatocellular carcinoma (HCC) tumours in ROCK1nc mice had higher grade steatosis, and more neutrophils and $CD8^+$ T cells relative to mice expressing wild-type ROCK1 (ROCK1wt), indicating that spontaneous tumour cell death also was more immunogenic. Since the induction of ICD has been proposed to be tumour-suppressive, the effects of two structurally distinct pharmacological ROCK inhibitors on HCC tumours was examined. Both fasudil and AT13148 significantly decreased tumour numbers and area, but neither treatment resulted in greater numbers of neutrophils or $CD8^+$ T cells to be recruited. In the context of acute DEN-induced liver damage, AT13148 reduced circulating platelet and lymphocyte numbers, and inhibited the recruitment of dendritic, natural killer and $CD8^+$ T cells to livers. These observations indicate that there is an important role for ROCK1 cleavage to limit immunogenic cell death which was not replicated by systemic administration of pharmacological ROCK inhibitors. As a result, adjuvant administration

of ROCK inhibitors with cancer therapeutics would be unlikely to result in therapeutic benefit by inducing ICD to increase anti-tumour immune responses.

Introduction

Apoptotic cell death is associated with profound morphological changes including cell contraction, blebbing, nuclear disintegration and apoptotic body release [2]. In addition, apoptotic cells display a variety of “find me” and “eat me” signals that aid in the efficient recognition and clearance of cell corpses by phagocytic cells including macrophages [3–5]. These events reduce the risk of cellular contents being released by dying cells in order to limit the induction of acute inflammatory and adaptive immune responses over time [6]. In the absence of efficient clearance of apoptotic cells, immunogenic cell death (ICD) may result in which the release of damage-associated molecular patterns (DAMPs) and induction of cytokines can promote the recruitment and activation of antigen-presenting cells and subsequent activation of cytotoxic T-lymphocyte (CTL) mediated adaptive immunity [7]. Although cancers typically employ several strategies to evade detection and/or destruction by the immune system, inducing tumour cell ICD can improve the efficacy of cancer therapeutic agents by promoting anti-tumour immunity [8,9]. Some anti-cancer agents act both by blocking essential targets in tumour cells and by inducing ICD [10]. In addition, the physical interventions of irradiation, photodynamic therapy and high hydrostatic pressure have all been shown to induce cancer cell ICD by promoting the release of DAMPs and the induction of pro-inflammatory cytokines [11]. Therefore, therapeutic agents that directly promote ICD could have beneficial effects for cancer treatment.

72 The biochemical processes induced by pro-apoptotic stimuli culminate in the
73 activation of executioner caspases that cleave substrate proteins at specific target
74 sequences [12]. We and others discovered that caspase cleavage of the ROCK1 protein
75 kinase at a highly conserved DETD sequence resulted in the generation of a
76 constitutively-active fragment [13,14]. Caspase-mediated ROCK1 activation led to
77 increased myosin light chain (MLC) phosphorylation and actin-myosin contraction that
78 were necessary for rapid cell contraction, membrane blebbing and nuclear fragmentation
79 during apoptosis [1,13,15]. Pharmacological inhibition of ROCK activity in apoptotic cells
80 was sufficient to block increased MLC phosphorylation, membrane blebbing and nuclear
81 disruption without affecting biochemical aspects of apoptotic cell death including caspase
82 activation, DNA fragmentation, cytochrome C release and phosphatidylserine
83 externalization [13,15,16]. A genetically modified mouse model in which a single amino
84 acid change in the DETD caspase cleavage site that rendered ROCK1 insensitive to
85 caspase cleavage revealed the obligatory role of ROCK1 cleavage and activation for MLC
86 phosphorylation, the generation of cellular contractile force and the morphological
87 aspects of apoptotic cell death [1]. Treatment of mice expressing the non-cleavable
88 ROCK1 (ROCK1nc) with the liver selective hepatotoxin diethylnitrosamine (DEN) [17] that
89 undergoes CYP2E1-mediated oxidation to become an active genotoxin [18] resulted in
90 greater acute liver damage and neutrophil recruitment relative to mice expressing wild-
91 type ROCK1 (ROCK1wt) [1]. Apoptotic ROCK1nc cells released more of the DAMP
92 protein high mobility group B1 (HMGB1) than ROCK1wt cells, and DEN-induced acute
93 liver damage and neutrophil recruitment could be significantly reduced by inhibiting
94 HMGB1 or its cognate pattern recognition receptor (PRR) toll-like receptor 4 (TLR4) [1].

95 Taken together, these findings indicated that the inability of cells to undergo typical
96 apoptotic morphological changes due to the absence of caspase-mediated ROCK1
97 activation induced a form of ICD.

98 DEN induction of hepatocyte apoptosis and tissue damage can progress to
99 hepatocellular carcinoma (HCC) over time [17]. While both ROCK genotypes developed
100 tumours 6 or 9 months after DEN treatment, there were fewer HCC tumours in ROCK1nc
101 mice at both time points [1]. These observations suggested that the ROCK1nc mutation
102 which affected apoptotic cell morphologies and resulted in acute hepatocyte ICD following
103 DEN-treatment could also have a tumour-suppressive effect. Furthermore, these results
104 raised the possibility that pharmacological ROCK inhibition could also have similar tumour
105 suppressive effects by inducing ICD.

106 In this study, we observed that the ROCK1nc mutation altered the typical
107 morphological changes of apoptotic hepatocytes *in vitro*, and resulted in greater induction
108 of pro-inflammatory cytokines in ROCK1nc mice relative to ROCK1wt mice following
109 acute DEN treatment, consistent with the absence of ROCK1 cleavage leading to ICD.
110 DEN-induced HCC tumours in ROCK1nc mice displayed higher grade steatosis, which
111 was accompanied by significantly more neutrophils and $CD8^+$ T cells relative to ROCK1wt
112 mice, while levels of $Foxp3^+$ regulatory T cells (Tregs) were not different. Taken together,
113 these results indicated that the ROCK1nc mutation induced immune responses that have
114 been associated with tumour suppression and improved patient outcomes [8]. To
115 determine if pharmacological ROCK inhibition could phenocopy the effect of the
116 ROCK1nc mutation, wild-type ROCK1 mice were treated with the ROCK inhibitors fasudil
117 [19] or AT13148 [20–22] following DEN-initiation of HCC. Although both ROCK inhibitors

118 significantly reduced HCC tumour numbers and areas, neither increased neutrophil or
119 $CD8^+$ T cell recruitment relative to vehicle controls. By examining the effect of AT13148
120 on acute DEN-induced liver damage, it was observed that the numbers of circulating
121 platelets and lymphocytes were decreased, as were the proportion of dendritic, natural
122 killer and $CD8^+$ T cells recruited to damaged livers. Taken together, these observations
123 indicate that the caspase-cleavage of ROCK1 is required to limit innate and adaptive
124 immune responses to acute DEN-induced liver damage and spontaneous apoptosis in
125 HCC tumours. However, potential therapeutic benefits from the tumour-suppressive
126 actions of the ROCK1nc mutation could not be recapitulated by systemic pharmacological
127 ROCK inhibition. As a result, it is unlikely that the addition of ROCK inhibitors as a cancer
128 therapy adjuvant would improve therapeutic efficacy by inducing ICD and promoting anti-
129 cancer immune responses. Nevertheless, ROCK inhibitor monotherapy did have a
130 significant effect on reducing HCC tumour growth, suggesting that there may be clinical
131 utility for ROCK inhibitors in the treatment of liver cancer, similar to the positive effects
132 observed in pre-clinical studies for other cancer types including pancreatic ductal
133 adenocarcinoma [22–24] and squamous cell carcinoma [25].

134

135 **Results**

136 ***Caspase cleavage of ROCK1 affects hepatocyte morphology, liver gene***
137 ***expression and cytokine release following genotoxin treatment***

138 The apoptotic death of mouse embryo fibroblasts (MEFs) homozygous for the ROCK1nc
139 genetic modification resulted in less contractile force generation relative to wild-type

140 MEFs, leading to fewer apoptotic blebs [1]. To determine if there were similar effects on
141 the apoptotic death of hepatocytes, primary hepatocytes from ROCK1wt and ROCK1nc
142 mice were isolated, treated with the apoptotic stimulus of the Bcl2 selective BH3 mimetic
143 ABT-199 (1 μM), then imaged using bright field microscopy at 3-minute time intervals.
144 While ROCK1wt hepatocytes underwent rapid and forceful contraction that produced
145 many blebs (Figure 1A, left panels; Video 1), apoptotic ROCK1nc hepatocytes were less
146 compact, had more residual contraction fibres and fewer apoptotic blebs (Figure 1A, right
147 panels; Video 2). Scanning electron microscopy revealed that the cell bodies of
148 ROCK1WT hepatocytes were studded with large blebs, while ROCK1nc were essentially
149 devoid of blebs and had large patches of membrane adjacent to the cell (Figure 1B).
150 Therefore, the ROCK1nc mutation that renders ROCK1 resistant to caspase mediated
151 proteolysis and activation similarly affected the apoptotic morphological features of
152 contraction and blebbing for hepatocytes and fibroblasts [1].

153 The liver-selective pro-hepatotoxin diethylnitrosamine (DEN) [17] can be
154 metabolized by CYP2E1 [18] to become genotoxic [26], resulting in hepatocyte apoptosis
155 and tissue damage that can progress to cirrhosis and hepatocellular carcinoma (HCC)
156 [17]. The toxic effects of DEN occur with high penetrance in male mice, with female mice
157 being relatively insensitive [17]. After intraperitoneal (IP) injection of 10 week old male
158 mice with 100 mg/kg DEN, haematoxylin and eosin (H&E) staining of livers isolated 72
159 hours later revealed markedly greater levels of steatosis in ROCK1nc mice compared to
160 livers from ROCK1wt mice (Figure 2A), consistent with previous observations [1]. RNA
161 was isolated from 4 untreated ROCK1wt and ROCK1nc livers, and from 4 ROCK1wt and
162 ROCK1nc livers 72 hours after DEN treatment, and polyA$^+$-enriched RNA was

163 sequenced. There were 2515 genes that were significantly altered in expression by at
164 least 1.5 fold (adjusted $p < 0.05$) between untreated and DEN treated ROCK1wt livers
165 (Figure 2–figure supplement 1A), and 1255 genes that were similarly altered in
166 expression between untreated and DEN treated ROCK1nc livers (Figure 2–figure
167 supplement 1B), of which 740 were in common (Figure 2B). The direction of change was
168 consistent for 96.5% of the 740 common genes (Figure 2–figure supplement 1C),
169 although the magnitude of positive and negative gene expression changes was
170 significantly greater for ROCK1wt than for ROCK1nc livers (Figure 2–figure supplement
171 1D). Gene set enrichment analysis revealed that there were four Reactome gene sets
172 (out of 1604 total gene sets) [27,28] that were significantly (nominal $p < 0.05$) altered in
173 both ROCK1wt and ROCK1nc livers (Figure 2C). In addition to the top hit "Transcriptional
174 Regulation by tp53" gene set that likely reflects the DNA damaging actions of DEN [29],
175 the next three gene sets were all related to immune signalling pathways. To determine if
176 there were differences in cytokine induction between ROCK1wt and ROCK1nc mice
177 following DEN treatment, the levels of 14 cytokines/chemokines were measured by
178 cytokine arrays. By comparing the fold-change induction of each cytokine/chemokine for
179 vehicle versus DEN treatment for each genotype, there was significantly greater induction
180 in ROCK1nc mice of interleukins (IL) IL-6, IL-1β, IL-10, tumour necrosis factor α (TNFα),
181 IL-12-p40, IL-4, IL-2, IL-1α, and C-C motif chemokine ligand 2 (CCL2) (Figure 2D). The
182 induction of IL-5, CCL3, IL12-p70, C-X-C motif chemokine ligand 9 (CXCL9) and
183 interferon γ (IFNγ) was not different between ROCK1wt and ROCK1nc mice, and no
184 cytokines/chemokines were induced to a significantly greater extent in ROCKwt mice
185 (Figure 2D). Taken together, these observations indicate preventing caspase-mediated

186 activation of ROCK1 leads to aberrant morphological changes during apoptotic
187 hepatocyte death and greater DEN-induced steatosis and inflammation.

188 ***Mutation of ROCK1 caspase cleavage site increases neutrophil, and CD3$^+$ and CD8$^+$***
189 ***T cell recruitment to hepatocellular carcinoma tumours.***

190 Treatment of 14 day old male mice with 400 µg DEN by IP injection results in the
191 development of HCC with high penetrance [1,17], with evidence of spontaneous
192 apoptosis in tumours [30]. ROCK1nc mice were previously shown to develop fewer HCC
193 tumours than ROCK1wt mice, suggesting that tumour development was affected by the
194 alterations in apoptotic cell morphologies due to absence of caspase-mediated ROCK1
195 activation [1]. Similar to there being more steatosis in ROCK1nc livers following acute
196 DEN-treatment [1], there was a significantly ($p < 0.001$, Chi-square test) higher proportion
197 of high grade (≥ 3) steatotic HCC tumours in ROCK1nc livers relative to ROCK1wt livers
198 (Figure 3A). In addition, steatosis was detectable in liver tumours of 12/12 ROCKnc mice
199 and only 10/12 ROCKwt mice. Despite the greater steatosis in ROCK1nc tumours, there
200 were no significant difference in biochemical markers of liver function and health between
201 ROCK1wt and ROCK1nc mice (Figure 3A–figure supplement 1A-H).
202 Immunohistochemical (IHC) analysis revealed that there were significantly more S100A9$^+$
203 neutrophils in ROCK1nc tumours relative to ROCK1wt tumours (Figure 3B), and no
204 difference in F4/80$^+$ macrophages between the genotypes (Figure 3C), comparable to the
205 observations for acute DEN treatment [1]. Since previous studies have reported that low
206 ratios of Foxp3$^+$ regulatory T cells (Tregs) to either CD3$^+$ or CD8$^+$ T cells were correlated
207 with better prognosis for patients with HCC [31–34], the levels of each cell types was
208 assessed in ROCK1wt and ROCK1nc HCC tumours. Both CD3$^+$ (Figure 4A) and CD8$^+$ T

209 cells (Figure 4B) were detected at significantly higher levels in ROCK1nc liver tumours
210 than in ROCK1wt tumours, while there was no difference in Foxp3^{+} Treg numbers (Figure
211 4C). These results indicate that the enhanced pro-inflammatory cytokine responses
212 observed in ROCK1nc mouse livers after acute DEN-treatment (Figure 2D) are paralleled
213 by greater CD8^{+} T cell responses in HCC tumours (Figures 3-4).

214 ***Pharmacological ROCK inhibition reduces DEN-induced liver tumour numbers***
215 ***without increased immune cell recruitment.***

216 A proposed cancer treatment strategy is to enable the immune system to more effectively
217 target cancers by increasing the immunogenicity of tumour cells by transforming
218 spontaneous or therapy-induced cell death from immunologically-silent apoptosis to a
219 more inflammatory necrotic-like form [6,35–37]. Results from the ROCK1nc mouse model
220 indicate that blocking caspase-induced ROCK1 activation leads to increased acute
221 inflammation (Figure 2D) that results in greater innate and adaptive immune responses
222 (Figures 3-4), which were correlated with reduced tumour numbers [1]. These
223 observations suggest that pharmacological ROCK inhibition could have a similar effect
224 as the ROCK1nc mutation in promoting tumour suppressive immune responses, which
225 could result in a novel clinical use for ROCK inhibitors as pro-immunogenic agents for
226 cancer therapy. To test this possibility, 14 day old male ROCK1wt mice were IP injected
227 with 400 µg DEN, and then at 10 weeks mice were orally administered either with water
228 vehicle or 2 mg of the ROCK inhibitor fasudil [19] twice daily until mice reached 41 weeks
229 (Figure 5A). Fasudil treatment had no significant effects on whole body, liver, lung or
230 spleen weights (Figure 5–figure supplement 1A-G). In addition, fasudil treatment had no
231 significant effects on blood haemoglobin levels or the numbers of circulating platelets,

232 white cells, lymphocytes or monocytes, but did result in a reduction in neutrophil numbers
233 (Figure 5–figure supplement 2A-F), and no effect on biochemical markers of liver health
234 and function except for decreased serum levels of aspartate aminotransferase (Figure 5–
235 figure supplement 2G-I). While liver tumours were observed in all mice for both treatment
236 groups (Figure 5B), tumour numbers (Figure 5C) and total tumour areas (Figure 5D) were
237 significantly lower in the fasudil treated mice. IHC analysis revealed no significant
238 differences in S100A9^{+} neutrophils (Figure 5E) in liver tumours. A trend towards fewer
239 CD8^{+} T cells in the livers of fasudil treated mice (Figure 5F) did not reach statistical
240 significance. To corroborate these observations, a comparable experiment substituted
241 the structurally unrelated ROCK inhibitor AT13148 [20–22] for fasudil. ROCK1wt mice
242 that had been injected IP at 14 days with 400 µg DEN were then orally administered three
243 times per week with either vehicle (10% DMSO, 1% Tween 20 in water) or 40 mg/kg
244 AT13148 until mice reached 41 weeks (Figure 6A). AT13148 treatment had no significant
245 effects on whole body, liver, lung or spleen weights (Figure 6–figure supplement 1A-G).
246 In addition, AT13148 had no significant effect on blood haemoglobin levels or the
247 numbers of circulating platelets, lymphocytes, monocytes or neutrophils, although white
248 cell numbers were significantly decreased (Figure 6–figure supplement 2A-F). AT13148
249 had no significant effects on biochemical markers of liver health and function (Figure 6–
250 figure supplement 2G-L). All livers from both treatment groups had tumours (Figure 6B),
251 although there were fewer tumours (Figure 6C) and smaller tumour areas (Figure 6D) for
252 the AT13148 treated mice. IHC analysis showed that there were no significant differences
253 in neutrophil numbers between the treatment groups (Figure 6E), but AT13148 treatment
254 resulted in fewer CD8^{+} T cells in liver tumours (Figure 6F). Although both ROCK inhibitors

255 fasudil and AT13148 had similar anti-tumour effects (Figures 5-6), neither treatment
256 increased neutrophil or $CD8^+$ T cell recruitment to tumours in contrast to the observations
257 in ROCK1nc mice (Figures 3-4).

258 To characterize the effect of ROCK inhibition on immune cell recruitment to the
259 liver in response to acute DEN treatment, 10 week old male ROCK1wt mice were orally
260 administered three times per week with either vehicle or 40 mg/kg AT13148 for 10 days,
261 with all mice receiving IP injections of 100 µg DEN on the 7th day. The addition of AT13148
262 with DEN did not result in significant differences in whole body or liver weight, or in blood
263 haemoglobin levels or numbers of circulating white cells, monocytes or neutrophils
264 relative to DEN treatment alone (Figure 7–figure supplement 1A-G). However, AT13148
265 did significantly reduce the number of circulating platelets (Figure 7A) and lymphocytes
266 (Figure 7B). Analysis of immune cell numbers in dissociated livers by flow cytometry
267 revealed that AT13148 significantly reduced the number of dendritic cells (Figure 7C), NK
268 cells (Figure 7D), $CD8^+$ T cells (Figure 7E) and Kupffer cells (Figure 7G) relative to vehicle
269 treated mice. The numbers of recruited macrophages, neutrophils, plasmacytoid dendritic
270 cells, $CD4^+$ T cells, Tregs, γδ T cells and NKT cells in DEN treated livers were not different
271 between vehicle and AT13148 treated mice (Figure 7-figure supplement 2A-H). These
272 findings indicate that the ROCK inhibitor AT13148 had an overall negative effect on
273 immune cell recruitment following acute DEN treatment.

274

275

276

277 **Discussion**

278 One of the hallmarks of cancer is the ability to evade destruction by the immune
279 system [38]. Immunoevasion is accomplished by a variety of means, but the strategy of
280 reactivating the immune system as an cancer therapeutic strategy has largely focussed
281 on the blocking the checkpoint inhibitor PD-1/PD-L1 and CTLA-4 pathways to enable
282 tumour-reactive T cells to muster effective antitumor responses [39]. An additional
283 strategy that is still in the process of becoming widely adopted is to intentionally induce
284 ICD to stimulate the immune system in concert with conventional targeted therapies [9].
285 The effect of ICD is to promote the action of dying cells as immunological adjuvants
286 through the release of DAMPs that promote the recruitment and activation of antigen-
287 presenting cells, ultimately resulting in activation of cytotoxic T lymphocyte-mediated
288 adaptive immunity and the establishment of immunological memory of tumour antigens
289 and neoantigens [7]. Cancer therapies are typically developed through an iterative
290 process that includes testing on established tumour cell lines *in vitro* and xenograft
291 tumours grown in immunocompromised mice to examine their anti-cancer effects, which
292 would not necessarily include assessments of their potential immunostimulatory or
293 immunosuppressive effects [40]. Nevertheless, some commonly used cancer
294 chemotherapies do in fact induce ICD including bleomycin, bortezomib, doxorubicin, and
295 oxaliplatin, although whether immunostimulation is a meaningful component of their
296 therapeutic mechanisms of action is not clear [40].

297 ROCK1nc mice express a mutated form of ROCK1 in which the caspase cleavage
298 site DETD (amino acids 1110-1113) was changed to DETA, making the protein resistant
299 to caspase cleavage [1,13]. The apoptotic death of ROCK1nc cells is characterized by

300 lower MLC phosphorylation, reduced cellular contractile force, altered morphologies and
301 greater HMGB1 release relative to cells expressing wild-type ROCK1 [1]. In ROCK1nc
302 mice, treatment with the hepatoxin DEN resulted in greater liver damage and neutrophil
303 recruitment than in ROCK1wt mice, both of which were reduced through inhibition of
304 HMGB1 or its receptor TLR4 [1]. In this study, acute DEN-induced liver damage was
305 associated with greater induction of pro-inflammatory cytokines in ROCK1nc mice
306 compared to ROCK1wt mice (Figure 2D). Taken together, these results are consistent
307 with cell death in ROCK1nc cells being immunogenic. In the long term, DEN-induced
308 fewer HCC tumours in ROCK1nc mice [1], with more high grade steatosis (Figure 3A)
309 and more neutrophil (Figure 3B) and $CD8^+$ T cells (Figure 4B) in ROCK1nc tumours
310 relative to ROCK1wt tumours. Levels of $F4/80^+$ macrophages (Figure 3C) and $Foxp3^+$
311 Treg cells (Figure 4C) were not significantly different between the genotypes. Clinical
312 studies in human HCC patients have previously determined that high $CD8^+$ T cells and/or
313 high $CD8^+/Foxp3^+$ ratios are associated with increased overall and disease-free survival
314 of HCC patients [32–34], suggesting that ICD in ROCK1nc tumours which resulted in high
315 $CD8^+$ T cell numbers and $CD8^+/Foxp3^+$ ratios induced tumour-suppressive immunity.
316 From a clinical perspective, the obvious question is whether pharmacological inhibition of
317 ROCK activity would provoke similar phenotypes.

318 Two structurally unrelated ROCK inhibitors, fasudil and AT13148, were selected
319 due to their previous efficacy in mouse tumour studies [22,24] and because both have
320 been shown to be safe for administration to human patients. Fasudil has been approved
321 and safely used in Japan and China for many years for the treatment of cerebral
322 vasospasm associated with subarachnoid hemorrhage [41], and there have been

323 additional proposed applications of fasudil as a therapy for neurodegenerative diseases
324 such as Amyotrophic Lateral Sclerosis [42,43] and cardiovascular diseases [44].
325 Development of AT13148 reached Phase I testing in patients with solid tumours [21].
326 Both fasudil and AT13148 reduced HCC tumour numbers and areas (Figures 5C-D, 6C-
327 D) indicating beneficial therapeutic actions, but neither led to increased numbers of
328 neutrophils or $CD8^+$ T cells in tumours relative to vehicle controls (Figures 5E-F, 6E-F).
329 In fact, AT13148 significantly reduced $CD8^+$ T cells in HCC tumours (Figure 6F), and
330 fasudil treatment resulted in a similar trend (Figure 5F). While the ROCK1nc mutation
331 only inhibits activation by caspase cleavage in apoptotic cells, pharmacological inhibitors
332 block activation resulting from caspase cleavage and RhoA binding, as well as reducing
333 basal kinase activity, of both ROCK1 and ROCK2 in all cells in the body [1,20,45]. The
334 actions of ROCK inhibitors that exceed the effect of the ROCK1nc mutation on kinase
335 activity, combined with the widespread targeting of apoptotic and non-apoptotic cells,
336 likely accounts for the differences observed for neutrophil and $CD8^+$ T cells in HCC
337 tumours between the genetic ROCK1nc modification and pharmacological ROCK
338 inhibition. Given the significant inhibitory effect of AT13148 on $CD8^+$ T cell numbers in
339 HCC tumours, the effects on immune cell recruitment in response to acute DEN damage
340 was examined. There were significantly fewer circulating platelets and lymphocytes in
341 AT13148 treated mice relative to vehicle controls (Figure 7A-B), while the numbers of
342 dendritic, NK and $CD8^+$ T cells recruited to ROCK1wt livers in response to DEN treatment
343 were reduced (Figures 7C-E). These observations are consistent with the reduction in
344 $CD8^+$ T cells found in HCC tumours in AT13148 treated mice (Figure 6F).

345 Apoptotic ROCK1nc cells released more of the DAMP protein HMGB1 and lactate
346 dehydrogenase (LDH), a cytosolic protein often used as a surrogate marker of cell death
347 [1], indicating that their cell death was more necrotic-like than the typical apoptotic death
348 of ROCK1wt cells. AT13148 development advanced to phase 1 clinical trials in patients
349 with solid tumours [21]. We previously showed that pharmacological ROCK inhibition
350 during early apoptosis reduced the release of LDH and the DAMP proteins Histones H1.2,
351 H2A, H2B, H3 and H4, S100-A4 and S100-A11, and heat shock proteins HSPA4, HSPA5,
352 HSP8, HSP90AA1, HSP90B1 and HSP90B2 relative to control apoptotic cells [16]. The
353 reduced release of cellular contents in ROCK inhibitor treated cells during early apoptosis
354 was attributed to decreased production of apoptotic bodies, which do not consistently re-
355 form impermeable membranes after detaching from apoptotic cell bodies, thus allowing
356 for leakage of their contents. As a result, a potential explanation for the differences in
357 neutrophil and $CD8^+$ T cell numbers in HCC tumours could be due to there being more
358 DAMP release in ROCK1nc mice than in ROCK inhibitor treated mice. An additional
359 possibility is that due to the central role of ROCK signalling in cell motility [46],
360 pharmacological ROCK inhibition impaired the ability of neutrophils and $CD8^+$ T cells to
361 migrate towards attractant stimuli.

362 Although the physical disruption of cells by irradiation, photodynamic therapy and
363 high hydrostatic pressure have been shown to induce ICD and could be used in
364 combination therapies to stimulate anti-tumour immune responses, altering the
365 morphological changes associated with apoptotic cell death by pharmacologically
366 blocking ROCK activity is not likely to be therapeutically beneficial. The ability of ROCK
367 inhibitors to reduce HCC tumour numbers and areas (Figures 5C-D, 6C-D) may be related

368 to their effects on blocking invasive tumour growth [22,24]. When the ability of ROCK
369 inhibitors to improve the efficacy of therapeutic agents by increasing tumour penetration
370 [23,47] is also considered along with their anti-metastatic properties [48], then there may
371 still be clinical benefits from the inclusion of ROCK inhibitors in HCC combination
372 therapies.

373

374 **Materials and Methods**

375 *Mouse Model*

376 ROCK1nc mice were generated at the Cancer Research UK Beatson Institute, and were
377 bred and maintained as described in [1]. All mouse experiments were approved by the
378 University of Glasgow College of Medicine, Veterinary and Life Sciences Research Ethics
379 Committee, and performed under a project license granted by the United Kingdom
380 government Home Office, in line with the Animals (Scientific Procedures) Act 1986 and
381 European Union Directive 2010/63/EU in a dedicated barriered facility. ROCK1wt and
382 ROCK1nc were backcrossed for more than 10 generations into the C57Bl/6J strain. Mice
383 were assigned to treatment groups by researchers who were not blinded with respect to
384 genotypes. For routine genotyping, all animals were ear notched at weaning and samples
385 sent to Transnetyx (Cordova, TN, US) genotyping service for analysis.

386 *Isolation of Hepatocytes*

387 Hepatocytes were isolated from male and female ROCK1nc and ROCK1wt mice by a
388 collagenase digestion and Percoll gradient method. Isolated cells were seeded on
389 collagen-coated plates. For coating plates with collagen (Corning, 354249), 50 mg/ml

390 collagen was prepared in water containing glacial acetic acid (6 µl in 5 ml water). Plates
391 were coated for 1 hour after which excess liquid was aspirated and plates left to dry in a
392 fume hood.

393 For hepatocyte isolation, mice were anesthetized before opening the thoracic and
394 peritoneal cavities. Livers were perfused with Liver Perfusion Media (Gibco,17701038) at
395 37°C via the right atrium and out through the portal vein. Once the liver became pale,
396 Perfusion Media was switched to Liver Digest Media (Gibco, 17703034). Digested livers
397 were excised, gall bladders removed, and then livers were transferred to dishes
398 containing Liver Perfusion Media. Livers were gently teased with forceps to release cells
399 into solution. Cell suspensions were then filtered through 70 µm cell strainers to remove
400 undigested tissue and connective tissue. Cells were centrifuged at 135 x g for 1 minute
401 and resuspended in 6 ml of hepatocyte media (William's E media (Gibco, 22551-022) with
402 3% fetal bovine serum (Gibco, 10270), 100 U/ml penicillin with 100 µg/ml streptomycin
403 (Gibco, 15140-122) and 2 mM L-glutamine (Gibco, 25030-032).

404 Hepatocytes were separated using a three-layer discontinuous Percoll (Sigma,
405 P1644) gradient. The Percoll density solutions used were; 1.12 g/ml, 1.08 g/ml and 1.06
406 g/ml. To make the 1.12 g/ml solution, 2.63 ml Percoll, 0.3 ml phosphate buffered saline
407 (PBS; 170 mM NaCl, 3.3 mM KCl, 1.8 mM Na_2HPO_4, 10.6 mM H_2PO_4) and 64.6 µl water
408 were mixed; for the 1.08 g/ml solution, 2.86 ml Percoll, 0.5 ml PBS and 1.63 ml water
409 were mixed; and for the 1.06 g/ml solution, 2.085 ml Percoll, 0.5 ml PBS and 2.42 ml
410 water were mixed. Percoll gradients were generated by layering 3 ml of the 1.12 g/ml
411 solution at the bottom over which 5 ml of the 1.08 g/ml solution was carefully layered
412 followed by 5 ml of the 1.06 g/ml solution. Over this, 6 ml of cell suspension was carefully

413 layered while avoiding gradient disturbance. The cell suspension was fractionated by
414 centrifugation without brakes at 750 x g for 20 minutes. After centrifugation, the layer of
415 cells between 1.06 g/ml and 1.08 g/ml that contained live hepatocytes was collected and
416 added to 10 ml of hepatocyte media. Cell suspensions were centrifuged at 135 x g for 1
417 minute. Cell pellets were then resuspended in hepatocyte media and seeded on collagen
418 coated plates for analysis.

419 *Time-lapse Microscopy of Hepatocytes*

420 ROCK1wt and ROCK1nc primary hepatocytes were plated on 6-well glass bottom dishes
421 pre-coated with collagen. Cells were serum-starved overnight prior to induction of
422 apoptosis with 1 μM ABT-199 (Selleckchem, S8048) diluted in serum-free media. Bright
423 field time-lapse microscopy images were acquired with a 10x objective using a Nikon TE
424 2000 microscope with a heated stage and 5% CO_2 gas line. Immediately after induction
425 of apoptosis, dishes were transferred to the microscope, 3-4 random positions were
426 chosen from each well and time lapse images were taken every 3 minutes for 18 hours.

427 *Scanning Electron Microscopy (SEM)*

428 Hepatocytes were cultured on collagen coated 10 mm glass cover slips in 24 well plates.
429 Apoptosis was induced using UVC radiation (254 nm wavelength at 0.3 J/cm^2) and cells
430 were processed for SEM at 24 hours post apoptosis induction. Cover slips were washed
431 twice in filtered PBS then fixed in 1.5% glutaraldehyde (Sigma, G5882) in 0.1 M sodium
432 cacodylate for 1 hour at room temperature. Samples were then washed twice in 0.1 M
433 sodium cacodylate and stored in 0.1 M sodium cacodylate. Cells were washed with
434 phosphate buffer (3 washes for 10 minutes), post-fixed in 1% Osmium Tetroxide/0.1M

435 Sodium Cacodylate buffer for 1 hour then washed for 3 x 10 minutes in distilled water.
436 Dehydration steps were through a graded ethanol series (30%, 50%, 70%, 90%) for 10
437 mins each, then 100% ethanol 4 times for 5 mins each. Samples were dried with
438 hexamethyldisilazane (Sigma, H4875) before coating with gold/palladium, and were
439 imaged on a JEOL 6400 Scanning Electron Microscope running at 10Kv. TIFF images
440 were captured using Olympus Scandium software at the Electron Microscopy Facility at
441 the University of Glasgow.

442 *Preparation and administration of substances*

443 To prepare diethylnitrosamine (DEN; Sigma, N0258), 100 ml of sterile PBS was injected
444 into the bottle containing 1 g of DEN to give a final concentration of 10 mg/ml. The
445 procedure was performed in the fume hood. For short-term studies assessing DEN-
446 induced hepatic injury, mice were treated with a single dose of DEN at 100 mg/kg body
447 weight by intraperitoneal injection.

448 To prepare fasudil, 1 g of fasudil (LC Laboratories, F-4660) was dissolved in 50 ml
449 distilled water giving a final concentration of 20 mg/ml. Fasudil was then aliquoted and
450 stored at -20°C until required for dosing. Mice were dosed with 100 µl (2 mg) fasudil twice
451 daily for the duration of the study.

452 To prepare AT13148 (Selleckchem, S7563), compound was dissolved in 89%
453 H_2O/10% (v/v) DMSO (Sigma, D2650)/1% (v/v) Tween 20 (Sigma, P1379) at a
454 concentration of 8 mg/ml. The dissolved drug was kept at 4°C for a maximum of 2 weeks.
455 Mice were dosed three times per week (Monday, Wednesday, Friday) for the duration of

456 studies performed. Mice were dosed initially with 30 mg/kg for the first two weeks, then
457 40 mg/kg thereafter.

458 *Tissue collection and fixation*

459 Animals were euthanized by carbon dioxide inhalation, weights recorded, and blood
460 collected for haematology or biochemistry analysis. Necropsy was performed
461 immediately to prevent tissue autolysis. Tissues collected were fixed for at least 24 hours
462 by immersing in 10% neutral buffered formalin. For acute liver studies, the left lobe of the
463 liver was routinely used for histological analysis and fixed in 10% neutral buffered
464 formalin. Small pieces from the median lobe were frozen using dry ice or collected in
465 RNALater for RNA analysis. The caudate lobe was frozen using dry ice for making
466 cryosections.

467 For DEN-induced hepatocellular carcinoma studies, mice were examined for
468 visible lesions in all organs, liver weights were recorded and the number of tumours
469 counted. Tumour foci were measured using digitised vernier callipers. Steatosis was
470 graded on H&E-stained sections based on semi-quantitative estimation of percentage of
471 steatotic hepatocytes, according to the following criteria: grade 0, less than 5%; grade 1,
472 5 to 25%; grade 2, 26 to 50%; grade 3, 51 to 75%; grade 4, more than 75%. Lungs were
473 also collected to analyse metastatic lesions. Tissue were either fixed in 10% neutral
474 buffered formalin for histological analysis or maintained in PBS until analysis. Fixed
475 tissues were then processed, paraffin embedded and sectioned by the Cancer Research
476 UK Beatson Institute Histology Service.

477 *Histology*

478 Paraffin-embedded tissue sections of 4 µm thickness were cut and routinely stained with
479 haematoxylin and eosin (H&E) by the Beatson Histology Service. Blank paraffin sections
480 were stored at 4° C until ready for use. Frozen liver tissue was embedded in OCT and cut
481 at 12 µm thickness and mounted on super-frost slides. Cryosections were stored at -80°C
482 until ready to be used.

483 *RNA isolation and sequencing*

484 RNA was isolated using the Qiagen RNasy Mini Kit according to the
485 manufacturer's instruction. RNA concentration and purity was determined using
486 NanoDrop 2000 spectrophotometer. RNA quality was confirmed using the Agilent RNA
487 Screen Tape assay and the Aligent 2200 TapeStation. Total RNA was used to generate
488 an oligo dT-enriched library with the Illumina TruSeq RNA Library Preparation kit v2.0.
489 Quality and quantity of the DNA library was assessed using an Agilent 2100 Bioanalyzer
490 and a Qubit (Thermo Fisher Scientific), respectively. The library was run on the Illumina
491 NextSeq 500 platform using the High Output 75 cycles kit (2 x 36 cycles, paired-end
492 reads, single index). RNAseq data were analysed by the Computational Biology
493 department at the CRUK Beatson Institute. Gene set enrichment analysis (GSEA) was
494 run using GSEA v4.1.0 for Windows [49].

495 Quality control checks of raw RNA-Seq data files were done with fastqc
496 (http://www.bioinformatics.babraham.ac.uk/projects/fastqc/) and fastq_screen
497 (http://www.bioinformatics.babraham.ac.uk/projects/fastq_screen/). RNA-Seq reads
498 were aligned to the mouse genome (GRCm38.75) using TopHat2 [50] and BAM files were
499 further processed with htseq_count

500 (http://www.huber.embl.de/users/anders/HTSeq/doc/count.html). Differential analysis of
501 count data was performed by the DESeq2 package [51].

502 *Multiplex Cytokine Analysis*

503 MILLIPLEX Multiplex Assays Using Luminex (Millipore, MCYTOMAG-70K) were used to
504 measure the levels of 15 cytokines (INF-γ, IL-1α, IL-1β, IL-2, IL-4, IL-5, IL-6, IL-10,
505 IL12p40, IL12p70, IL-17, CCL2, CCL3, CXCL9, TNFα). Serum levels of these cytokines
506 were analysed using the Mouse Cytokine/Chemokine Magnetic Bead Panel Kit following
507 manufacturer's instructions. Briefly, 200 µl of wash buffer was added to each well of 96-
508 well plates, which were sealed and mixed on a plate shaker for 10 minutes at room
509 temperature after which the wash buffer was decanted. Inverting the plates and tapping
510 them onto absorbent towels removed residual wash buffer. 25 µl of standards or controls
511 were added to the appropriate wells and 25 µl of assay buffer was added to the sample
512 wells. 25 µl of serum matrix was added to the background, control and standard wells.
513 25 µl of serum samples diluted 1:2 in assay buffer was added to the sample wells. All
514 serum samples were measured in duplicate. 25 µl of premixed magnetic beads
515 conjugated to antibodies for all 15 analytes were added to each well. Plates were sealed,
516 protected from light and incubated overnight at 4° C on a plate shaker. This was followed
517 by a wash step (two times with 200 µl of wash buffer) on a magnetic plate washer. 25 µl
518 of detection antibodies was added to each well, and plates were sealed and incubated
519 with agitation for 1 hour at room temperature. Streptavidin-phycoerythrin (25 µl) was
520 added to each well, and plates were sealed and incubated with agitation for another 30
521 minutes at room temperature, followed by a final wash step. Magnetic beads were then

522 re-suspended in sheath fluid and assayed on a Luminex 200 analyser using xPOTENT
523 software.

524 *Immunohistochemistry*

525 Immunohistochemistry was routinely performed on 4 µm thick formalin-fixed paraffin-
526 embedded (FFPE) sections. Sections were deparaffinised in xylene (3 washes of 5
527 minutes each) and rehydrated through decreasing concentrations of ethanol (2 washes
528 of 3 minutes each in 100% ethanol, 1 wash for 3 minutes in 70% ethanol). Slides were
529 then washed in distilled water (dH2O). To unmask antigens, slides were boiled at 98° C
530 in a water bath (WB) for the specified time in antigen retrieval buffer. The buffers used
531 varied with the antibody (Table 1). If Proteinase K (Dako, S2032) was used as the retrieval
532 agent, then the slides were incubated at room temperature for the specified time (Table
533 1). Slides were left to cool down to room temperature for at least 30 minutes and then
534 rinsed in distilled water. Endogenous peroxidase activity was quenched by incubating
535 sections in 3 % H_2O_2 (Fisher, 10687022) in PBS for 10 minutes. After slides were rinsed
536 once in distilled water and once in Tris-buffered saline + Tween 20 (TBST; 20 mM Tris-
537 HCL pH 7.5, 136 mM NaCl, 0.1% (v/v) Tween 20), sections were blocked using blocking
538 solution containing 5% serum (depending on the species in which the secondary antibody
539 was raised) in TBST for 30 minutes at room temperature. Primary antibody diluted in
540 blocking solution was added to the slides and kept in a humidified chamber for the
541 specified time. Primary antibody dilutions and incubation times are indicated in Table 1.
542 Slides were rinsed three times in TBST to remove excess/unbound primary antibody.
543 HRP-labelled secondary antibodies were added to the slides and incubated at room
544 temperature for 30 minutes at room temperature. For secondary antibody staining, either

545 ImmPRESS kits (anti-goat, MP-7405; anti-rat, MP-7444) or Envision+ Reagents (Dako:
546 rabbit, K4002) were used. Slides were rinsed again three times in TBST before staining
547 with 3, 3'-diaminobenzidine tetrahydrochloride (DAB; Dako, K3467), as chromogen.
548 Sections were incubated with DAB solution until brown colour develops and the slides
549 were immediately transferred to TBST to stop the reaction.

550 **Table 1. Antigen retrieval methods, primary antibodies with dilutions, and**
551 **incubation conditions for IHC.** Citrate buffer (10 mM Sodium citrate, 0.05% (v/v) Tween
552 20). WB = water bath. RT = room temperature.

Antigen (clone)	Species	Supplier (Catalogue Number)	Antigen Retrieval Solution	Retrieval Method	Antibody Dilution; Time & Temperature
CD3 (SP7)	Rabbit	Vector (VP-RM01)	Citrate buffer pH 6	WB; 98°C; 25 min	1:75; 35 min, RT
F4/80 (Cl:A3-1)	Rat	Abcam (ab6640)	Proteinase K	10 min at RT	1:400; 35 min; RT
Foxp3 (FJK-16s)	Rat	eBioscience (14-5773-80)	Tris-EDTA buffer pH 9	WB; 98°C; 20 min	1:50; O/N; 4°C
S100A9 (M-19)	Goat	Santa Cruz (sc-8115)	Citrate buffer pH 6	WB; 98°C; 25 min	1:1000; 35 min; RT
CD8 (4SM15)	Rat	eBioscience (14-0808-82)	Tris-EDTA buffer pH 9	WB; 98°C; 20 min	1:500; 35 min; RT

553

554 For counterstaining, slides were rinsed in distilled water and then stained with
555 haematoxylin for 1 minute. After rinsing in distilled water, the slides were then transferred
556 to Scots tap water for 1 minute or until blue colour developed to the desired intensity.
557 Slides were rinsed in distilled water and the sections were dehydrated using increasing
558 concentrations of ethanol (1 wash for 3 minutes in 70% ethanol, 2 washes of 3 minutes
559 each in 100% ethanol). Slides were then cleared by three washes in xylene for 3-minutes

560 each, before mounting with DPX mountant (Sigma, 44581). In all staining experiments,
561 omitting the primary antibody on one slide served as the negative control. Sections were
562 analysed using bright field microscope (Olympus BX51) and representative images were
563 obtained at different magnifications.

564 *Immunofluorescence staining of frozen sections*

565 Immunofluorescence staining of cryosections was performed on 12 µm thick
566 cryosections. Tissue sections were fixed by immersing the slides in pre-cooled acetone
567 (-20°C) for 10 minutes. Slides were removed from fixative and acetone was allowed to
568 evaporate from the tissue sections for 20 minutes. After slides were rinsed in PBS,
569 cryosections were blocked in blocking buffer (5% serum in PBS) for 1 hour at room
570 temperature. Anti-CD8 primary antibody diluted in blocking buffer (1:100) was added to
571 the slides and kept in a humidified chamber for 2 hours at room temperature. Slides were
572 rinsed twice in PBS before adding Alexa Fluor 594 conjugated goat anti-rat secondary
573 antibody (ThermoFisher Scientific, A48264) diluted 1:500 in blocking buffer and incubated
574 for 1 hour at room temperature. Slides were then rinsed three times in PBS before
575 mounting with Vectashield DAPI hard set (Vector, H-1500). Cryosections were analysed
576 using fluorescence microscope (Olympus BX51) and images were obtained at 20x
577 magnification.

578 *Hepatocellular carcinoma induction*

579 Male mice were injected intraperitoneally (IP) with DEN as a single 40 µl dose (400 µg,
580 equates to ~10 µl/g) at 14 days old. Mice were checked at regular intervals for general
581 health and signs related to hepatocellular carcinoma such as hepatomegaly (swollen

582 abdomen), pain (hunched, high gait), weight loss (pinched shoulders) or reduced mobility.
583 The experimental end point was defined as 41 weeks, or in the event of development of
584 clinical signs, at which point mice were humanely culled and samples collected. Mouse
585 data such as body weight and organ weight were recorded, liver tumours were counted
586 and measured using calipers, and lungs and spleen were assessed for metastases. Blood
587 samples were additionally taken for analysis of haematological parameters and liver
588 function tests. For FFPE samples, tissues were collected and placed directly into 10%
589 neutral buffered formalin solution. Samples were placed on a rocker for 24 hours then
590 moved to a 70% ethanol solution until paraffin embedding. Tumour areas were calculated
591 using the following formula; Area = π x (Length/2) x (Width/2)

592 *Haematology*

593 Mice were euthanized by carbon dioxide inhalation and blood samples were collected via
594 cardiac puncture in potassium-EDTA tubes. Haematology analysis was performed by the
595 Clinical Pathology Lab at the Veterinary School (University of Glasgow).

596 *Liver Function*

597 Mice were euthanized by carbon dioxide inhalation and blood samples were collected via
598 cardiac puncture in 1.5 ml microcentrifuge tubes. Blood was allowed to clot at room
599 temperature for at least 30 minutes and then centrifuged at 1500 x g for 15 min at 4° C.
600 The resulting supernatant (serum) was transferred to fresh tubes for analysis. If the serum
601 samples were not analysed immediately, they were aliquoted and stored at -20° C until
602 ready for analysis. Liver function tests were performed by the Clinical Pathology Lab at
603 the Veterinary School (University of Glasgow), where serum concentrations of alanine

604 transaminase, total bilirubin, alkaline phosphatase, aspartate aminotransferase, total
605 protein, albumin and globulin were determined using an automated analyser.

606 *Flow Cytometry*

607 Cell suspensions were generated from mouse livers by first perfusing livers with PBS,
608 then dissecting them and placing into ice cold PBS. The liver tissues were dissociated
609 using scissors and incubated in a solution of 5 ml PBS containing 1 mg/ml collagenase D
610 (Millipore, 11088858001), 0.5 mg/ml dispase (Millipore, D4818) and 0.1 mg/ml
611 collagenase P (Millipore, 11213857001) at 40°C for 30 minutes shaking at 750 rpm. The
612 cell suspensions were then diluted in 45 ml RPMI 1640 (Gibco, 31870-025) and passed
613 through a 70 μM filter twice. The suspensions were then spun at 300 x g for 5 minutes
614 and resuspended in red blood cell (RBC) lysis buffer (Biolegend, 420302) for 5 minutes.
615 Following termination or RBC lysis in PBS, the suspensions were then spun down and
616 resuspended in PBS.

617 2.5×10^6 cells were stained in a volume of 100 μl unless otherwise stated. Cell
618 suspensions were incubated in Zombie NIR live dead dye (Biolegend, 423106) at 1:250
619 in PBS at room temperature for 20 minutes. Suspensions were spun at 300 x g for 3
620 minutes and washed twice in PBS. Suspensions were then incubated in Fc block at 1:250
621 in FACS buffer (PBS with 2% (v/v) FBS, 0.5% (w/v) sodium azide, 0.2 mM EDTA) for 20
622 minutes at room temperature then washed twice in FACS buffer. Cells were stained with
623 antibodies for 30 minutes at room temperature (Table 2). Cells were then spun down and
624 washed twice in FACS buffer. Secondary staining containing secondary antibodies and/or
625 streptavidin fluorophore conjugate was then performed in FACS buffer at room
626 temperature for 30 minutes. Cells were again spun down and washed twice in FACS

627 buffer. Cells were then resuspended in FACS buffer and an equal volume 4%
628 paraformaldehyde/PBS (final concentration 2%) was added for fixation.

629 Samples were analysed and data collected using an Attune NxT acoustic focusing
630 flow cytometer. Post-acquisition analysis was performed using FlowJo v10 software.

631 **Table 2. Liver flow cytometry staining panel**

Lymphoid Panel				Myeloid Panel			
Antigen (clone)	**Supplier**	**Dilu-tion**	**Fluoro-phore**	**Antigen (clone)**	**Supplier**	**Dilu-tion**	**Fluoro-phore**
B220 (RA3-6B2)	Biolegend	1:200	PerCPCy5.5	CD11b (M1/70)	Biolegend	1:200	BV570
CD3 (17A2)	Biolegend	1:200	FITC	CD11c (N418)	Biolegend	1:200	BV711
CD4 (RN4-5)	eBio-science	1:200	SB600	CD45 (30-F11)	Biolegend	1:200	BV510
CD8 (53-6.7)	Biolegend	1:200	PECy7	CD115 (AFS98)	Biolegend	1:100	BV421
CD19 (6D5)	Biolegend	1:200	PE	Clec4f	Biolegend	1:100	Goat/AF594
CD25 (PC61)	Biolegend	1:100	AF700	F4/80 (BM8)	Biolegend	1:100	Biotin/PE
CD45 (30-F11)	Biolegend	1:200	BV510	Ly6C (HK1.4)	Biolegend	1:400	PECy7
FoxP3 (MF14)	Biolegend	1:100	AF647	Ly6G (1A8)	Biolegend	1:200	AF700
NK1.1 (PK136)	Biolegend	1:200	BV711	MHCII (M5/114.15.2)	Biolegend	1:500	FITC
TCRβ (A57-597)	Biolegend	1:100	BV421	PDCA1 (927)	Biolegend	1:100	PerCPCy5.5
TCRγδ (GL3)	Biolegend	1:100	Biotin/AF594	Siglec H (551)	Biolegend	1:100	APC

632

633 *Statistical Analysis*

634 Graphpad Prism 9 software was used for statistical analysis of data and generation of
635 graphs. The specific test used for analysis is stated in each figure legend.

636

637 **Acknowledgements**

638 This study was funded the Canadian Institutes of Health Research (PJT-169125), Canada
639 Research Chairs Program (950-231665), and by Cancer Research UK institutional
640 funding to the CRUK Beatson Institute (A10419, A17196) and to the Olson lab (A18276).
641 Thanks to the Cancer Research UK Beatson Institute Biological and Histology Services,
642 as well as the University of Glasgow Veterinary School Clinical Pathology Laboratory.

643

644 **Competing interests**

645 The authors declare that they have no conflict of interest.

646

647 **Dataset availability**

648 RNA sequencing data is available upon request.

649

650 **References**

651 1. Julian, L.; Naylor, G.; Wickman, G.R.; Rath, N.; Castino, G.; Stevenson, D.;
652 Bryson, S.; Munro, J.; McGarry, L.; Mullin, M.; et al. Defective Apoptotic Cell
653 Contractility Provokes Sterile Inflammation, Leading to Liver Damage and
654 Tumour Suppression. *Elife* **2021**, *10*, doi:10.7554/eLife.61983.

655 2. Wickman, G.; Julian, L.; Olson, M.F. How Apoptotic Cells Aid in the Removal of

656 Their Own Cold Dead Bodies. *Cell Death Differ.* **2012**, *19*, 735–742,
657 doi:10.1038/cdd.2012.25.

658 3. Elliott, M.R.; Ravichandran, K.S. Clearance of Apoptotic Cells: Implications in
659 Health and Disease. *J. Cell Biol.* **2010**, *189*, 1059–1070.

660 4. Boada-Romero, E.; Martinez, J.; Heckmann, B.L.; Green, D.R. The Clearance of
661 Dead Cells by Efferocytosis. *Nat. Rev. Mol. Cell Biol.* **2020**, *21*, 398–414,
662 doi:10.1038/s41580-020-0232-1.

663 5. Nagata, S. Apoptosis and Clearance of Apoptotic Cells. *Annu. Rev. Immunol.*
664 **2018**, *36*, 489–517, doi:10.1146/annurev-immunol-042617-053010.

665 6. Kroemer, G.; Galassi, C.; Zitvogel, L.; Galluzzi, L. Immunogenic Cell Stress and
666 Death. *Nat. Immunol.* **2022**, doi:10.1038/s41590-022-01132-2.

667 7. Galluzzi, L.; Vitale, I.; Warren, S.; Adjemian, S.; Agostinis, P.; Martinez, A.B.;
668 Chan, T.A.; Coukos, G.; Demaria, S.; Deutsch, E.; et al. Consensus Guidelines
669 for the Definition, Detection and Interpretation of Immunogenic Cell Death. *J.*
670 *Immunother. cancer* **2020**, *8*, doi:10.1136/jitc-2019-000337.

671 8. Galluzzi, L.; Zitvogel, L.; Kroemer, G. Immunological Mechanisms Underneath the
672 Efficacy of Cancer Therapy. *Cancer Immunol. Res.* **2016**, *4*, 895–902,
673 doi:10.1158/2326-6066.CIR-16-0197.

674 9. Petroni, G.; Buqué, A.; Zitvogel, L.; Kroemer, G.; Galluzzi, L. Immunomodulation
675 by Targeted Anticancer Agents. *Cancer Cell* **2021**, *39*, 310–345,
676 doi:https://doi.org/10.1016/j.ccell.2020.11.009.

677 10. Hossain, D.M.S.; Javaid, S.; Cai, M.; Zhang, C.; Sawant, A.; Hinton, M.; Sathe,
678 M.; Grein, J.; Blumenschein, W.; Pinheiro, E.M.; et al. Dinaciclib Induces
679 Immunogenic Cell Death and Enhances Anti-PD1–Mediated Tumor Suppression.
680 *J. Clin. Invest.* **2018**, *128*, 644–654, doi:10.1172/JCI94586.

681 11. Galluzzi, L.; Buqué, A.; Kepp, O.; Zitvogel, L.; Kroemer, G. Immunogenic Cell
682 Death in Cancer and Infectious Disease. *Nat. Rev. Immunol.* **2017**, *17*, 97–111,
683 doi:http://dx.doi.org/10.1038/nri.2016.107.

684 12. Earnshaw, W.C.; Martins, L.M.; Kaufmann, S.H. Mammalian Caspases: Structure,
685 Activation, Substrates, and Functions during Apoptosis. *Annu Rev Biochem* **1999**,
686 *68*, 383–424.

687 13. Coleman, M.L.; Sahai, E.A.; Yeo, M.; Bosch, M.; Dewar, A.; Olson, M.F.
688 Membrane Blebbing during Apoptosis Results from Caspase-Mediated Activation
689 of ROCK I. *Nat. Cell Biol.* **2001**, *3*, 339–345, doi:10.1038/35070009.

690 14. Sebbagh, M.; Renvoize, C.; Hamelin, J.; Riche, N.; Bertoglio, J.; Breard, J.
691 Caspase-3-Mediated Cleavage of ROCK I Induces MLC Phosphorylation and
692 Apoptotic Membrane Blebbing. *Nat. Cell Biol.* **2001**, *3*, 346–352.

693 15. Croft, D.R.; Coleman, M.L.; Li, S.; Robertson, D.; Sullivan, T.; Stewart, C.L.;
694 Olson, M.F. Actin-Myosin-Based Contraction Is Responsible for Apoptotic Nuclear
695 Disintegration. *J. Cell Biol.* **2005**, *168*, 245–255, doi:10.1083/jcb.200409049.

696 16. Wickman, G.R.; Julian, L.; Mardilovich, K.; Schumacher, S.; Munro, J.; Rath, N.;
697 Zander, S. AL; Mleczak, A.; Sumpton, D.; Morrice, N.; et al. Blebs Produced by
698 Actin-Myosin Contraction during Apoptosis Release Damage-Associated

699 Molecular Pattern Proteins before Secondary Necrosis Occurs. *Cell Death Differ.*
700 **2013**, *20*, 1293–1305, doi:10.1038/cdd.2013.69.

701 17. Tolba, R.; Kraus, T.; Liedtke, C.; Schwarz, M.; Weiskirchen, R. Diethylnitrosamine
702 (DEN)-Induced Carcinogenic Liver Injury in Mice. *Lab. Anim.* **2015**, *49*, 59–69,
703 doi:10.1177/0023677215570086.

704 18. Kang, J.S.; Wanibuchi, H.; Morimura, K.; Gonzalez, F.J.; Fukushima, S. Role of
705 CYP2E1 in Diethylnitrosamine-Induced Hepatocarcinogenesis In Vivo. *Cancer*
706 *Res.* **2007**, *67*, 11141–11146, doi:10.1158/0008-5472.CAN-07-1369.

707 19. Nagumo, H.; Sasaki, Y.; Ono, Y.; Okamoto, H.; Seto, M.; Takuwa, Y. Rho Kinase
708 Inhibitor HA-1077 Prevents Rho-Mediated Myosin Phosphatase Inhibition in
709 Smooth Muscle Cells. *Am. J. Physiol. Physiol.* **2000**, *278*, C57–C65,
710 doi:10.1152/ajpcell.2000.278.1.C57.

711 20. Sadok, A.; McCarthy, A.; Caldwell, J.; Collins, I.; Garrett, M.D.; Yeo, M.; Hooper,
712 S.; Sahai, E.; Kuemper, S.; Mardakheh, F.K.; et al. Rho Kinase Inhibitors Block
713 Melanoma Cell Migration and Inhibit Metastasis. *Cancer Res.* **2015**, *75*, 2272–
714 2284, doi:10.1158/0008-5472.CAN-14-2156.

715 21. McLeod, R.; Kumar, R.; Papadatos-Pastos, D.; Mateo, J.; Brown, J.S.; Garces,
716 A.H.I.; Ruddle, R.; Decordova, S.; Jueliger, S.; Ferraldeschi, R.; et al. First-in-
717 Human Study of AT13148, a Dual ROCK-AKT Inhibitor in Patients with Solid
718 Tumors. *Clin. Cancer Res.* **2020**, *26*, 4777–4784, doi:10.1158/1078-0432.CCR-
719 20-0700.

720 22. Rath, N.; Munro, J.; Cutiongco, M.F.; Jagiełło, A.; Gadegaard, N.; McGarry, L.;

721 Unbekandt, M.; Michalopoulou, E.; Kamphorst, J.J.; Sumpton, D.; et al. Rho
722 Kinase Inhibition by AT13148 Blocks Pancreatic Ductal Adenocarcinoma Invasion
723 and Tumor Growth. *Cancer Res.* **2018**, *78*, 3321–3336, doi:10.1158/0008-
724 5472.CAN-17-1339.

725 23. Vennin, C.; Rath, N.; Pajic, M.; Olson, M.F.; Timpson, P. Targeting ROCK Activity
726 to Disrupt and Prime Pancreatic Cancer for Chemotherapy. *Small GTPases* **2020**,
727 *11*, 45–52, doi:10.1080/21541248.2017.1345712.

728 24. Rath, N.; Morton, J.P.; Julian, L.; Helbig, L.; Kadir, S.; McGhee, E.J.; Anderson,
729 K.I.; Kalna, G.; Mullin, M.; Pinho, A. V; et al. ROCK Signaling Promotes Collagen
730 Remodeling to Facilitate Invasive Pancreatic Ductal Adenocarcinoma Tumor Cell
731 Growth. *EMBO Mol Med* **2017**, *9*, 198–218, doi:10.15252/emmm.201606743.

732 25. Samuel, M.; Lopez, J.; McGhee, E.; Croft, D.; Strachan, D.; Timpson, P.; Munro,
733 J.; Schröder, E.; Zhou, J.; Brunton, V.; et al. Actomyosin-Mediated Cellular
734 Tension Drives Increased Tissue Stiffness and β-Catenin Activation to Induce
735 Epidermal Hyperplasia and Tumor Growth. *Cancer Cell* **2011**, *19*,
736 doi:10.1016/j.ccr.2011.05.008.

737 26. Bakiri, L.; Wagner, E.F. Mouse Models for Liver Cancer. *Mol. Oncol.* **2013**, *7*,
738 206–223, doi:https://doi.org/10.1016/j.molonc.2013.01.005.

739 27. Fabregat, A.; Jupe, S.; Matthews, L.; Sidiropoulos, K.; Gillespie, M.; Garapati, P.;
740 Haw, R.; Jassal, B.; Korninger, F.; May, B.; et al. The Reactome Pathway
741 Knowledgebase. *Nucleic Acids Res* **2018**, *46*, D649–D655,
742 doi:10.1093/nar/gkx1132.

743 28. Fabregat, A.; Sidiropoulos, K.; Viteri, G.; Marin-Garcia, P.; Ping, P.; Stein, L.;
744 D'Eustachio, P.; Hermjakob, H. Reactome Diagram Viewer: Data Structures and
745 Strategies to Boost Performance. *Bioinformatics* **2018**, *34*, 1208–1214,
746 doi:10.1093/bioinformatics/btx752.

747 29. Williams, G.M.; Iatropoulos, M.J.; Wang, C.X.; Ali, N.; Rivenson, A.; Peterson,
748 L.A.; Schulz, C.; Gebhardt, R. Diethylnitrosamine Exposure-Responses for DNA
749 Damage, Centrilobular Cytotoxicity, Cell Proliferation and Carcinogenesis in Rat
750 Liver Exhibit Some Non-Linearities. *Carcinogenesis* **1996**, *17*, 2253–2258,
751 doi:10.1093/carcin/17.10.2253.

752 30. Memon, A.; Pyao, Y.; Jung, Y.; Lee, J. Il; Lee, W.K. A Modified Protocol of
753 Diethylnitrosamine Administration in Mice to Model Hepatocellular Carcinoma. *Int.*
754 *J. Mol. Sci.* **2020**, *21*, 5461, doi:10.3390/ijms21155461.

755 31. Yao, W.; He, J.C.; Yang, Y.; Wang, J.M.; Qian, Y.W.; Yang, T.; Ji, L. The
756 Prognostic Value of Tumor-Infiltrating Lymphocytes in Hepatocellular Carcinoma:
757 A Systematic Review and Meta-Analysis. *Sci. Rep.* **2017**, *7*, 7525,
758 doi:10.1038/s41598-017-08128-1.

759 32. Mathai, A.M.; Kapadia, M.J.; Alexander, J.; Kernochan, L.E.; Swanson, P.E.; Yeh,
760 M.M. Role of Foxp3-Positive Tumor-Infiltrating Lymphocytes in the Histologic
761 Features and Clinical Outcomes of Hepatocellular Carcinoma. *Am. J. Surg.*
762 *Pathol.* **2012**, doi:10.1097/PAS.0b013e31824e9b7c.

763 33. Fu, J.; Xu, D.; Liu, Z.; Shi, M.; Zhao, P.; Fu, B.; Zhang, Z.; Yang, H.; Zhang, H.;
764 Zhou, C.; et al. Increased Regulatory T Cells Correlate With CD8 T-Cell

765 Impairment and Poor Survival in Hepatocellular Carcinoma Patients.
766 *Gastroenterology* **2007**, *132*, 2328–2339, doi:10.1053/j.gastro.2007.03.102.

767 34. Xu, X.; Tan, Y.; Qian, Y.; Xue, W.; Wang, Y.; Du, J.; Jin, L.; Ding, W.
768 Clinicopathologic and Prognostic Significance of Tumor-Infiltrating CD8+ T Cells
769 in Patients with Hepatocellular Carcinoma: A Meta-Analysis. *Medicine (Baltimore).*
770 **2019**, *98*, e13923.

771 35. Green, D.R.; Ferguson, T.; Zitvogel, L.; Kroemer, G. Immunogenic and
772 Tolerogenic Cell Death. *Nat Rev Immunol* **2009**, *9*, 353–363, doi:10.1038/nri2545.

773 36. Kroemer, G.; Galluzzi, L.; Kepp, O.; Zitvogel, L. Immunogenic Cell Death in
774 Cancer Therapy. *Annu Rev Immunol* **2013**, *31*, 51–72, doi:10.1146/annurev-
775 immunol-032712-100008.

776 37. Galluzzi, L.; Senovilla, L.; Zitvogel, L.; Kroemer, G. The Secret Ally:
777 Immunostimulation by Anticancer Drugs. *Nat. Rev. Drug Discov.* **2012**, *11*, 215,
778 doi:10.1038/nrd3626.

779 38. Hanahan, D.; Weinberg, R.A. Hallmarks of Cancer: The Next Generation. *Cell*
780 **2011**, *144*, 646–674, doi:https://doi.org/10.1016/j.cell.2011.02.013.

781 39. Wei, S.C.; Duffy, C.R.; Allison, J.P. Fundamental Mechanisms of Immune
782 Checkpoint Blockade Therapy. *Cancer Discov.* **2018**, *8*, 1069–1086,
783 doi:10.1158/2159-8290.CD-18-0367.

784 40. Galluzzi, L.; Buqué, A.; Kepp, O.; Zitvogel, L.; Kroemer, G. Immunological Effects
785 of Conventional Chemotherapy and Targeted Anticancer Agents. *Cancer Cell*

786 **2015**, *28*, 690–714, doi:https://doi.org/10.1016/j.ccell.2015.10.012.

787 41. Zhao, J.; Zhou, D.; Guo, J.; Ren, Z.; Zhou, L.; Wang, S.; Xu, B.; Wang, R. Effect
788 of Fasudil Hydrochloride, a Protein Kinase Inhibitor, on Cerebral Vasospasm and
789 Delayed Cerebral Ischemic Symptoms After Aneurysmal Subarachnoid
790 Hemorrhage; Results of a Randomized Trial of Fasudil Hydrochloride Versus
791 Nimodipine. *Neurol. Med. Chir. (Tokyo).* **2006**, *46*, 421–428,
792 doi:10.2176/nmc.46.421.

793 42. Koch, J.C.; Kuttler, J.; Maass, F.; Lengenfeld, T.; Zielke, E.; Bähr, M.; Lingor, P.
794 Compassionate Use of the ROCK Inhibitor Fasudil in Three Patients With
795 Amyotrophic Lateral Sclerosis. *Front. Neurol.* **2020**, *11*, 173,
796 doi:10.3389/fneur.2020.00173.

797 43. Koch, J.C.; Tatenhorst, L.; Roser, A.-E.; Saal, K.-A.; Tönges, L.; Lingor, P. ROCK
798 Inhibition in Models of Neurodegeneration and Its Potential for Clinical
799 Translation. *Pharmacol. Ther.* **2018**, *189*, 1–21,
800 doi:https://doi.org/10.1016/j.pharmthera.2018.03.008.

801 44. Satoh, K.; Fukumoto, Y.; Shimokawa, H. Rho-Kinase: Important New Therapeutic
802 Target in Cardiovascular Diseases. *Am. J. Physiol. - Hear. Circ. Physiol.* **2011**,
803 *301*, H287–H296.

804 45. Lee, J.H.; Zheng, Y.; von Bornstadt, D.; Wei, Y.; Balcioglu, A.; Daneshmand, A.;
805 Yalcin, N.; Yu, E.; Herisson, F.; Atalay, Y.B.; et al. Selective ROCK2 Inhibition In
806 Focal Cerebral Ischemia. *Ann. Clin. Transl. Neurol.* **2014**, *1*, 2–14,
807 doi:10.1002/acn3.19.

808 46. Olson, M.F.; Sahai, E. The Actin Cytoskeleton in Cancer Cell Motility. *Clin. Exp.*
809 *Metastasis* **2009**, *26*, 273–287, doi:10.1007/s10585-008-9174-2.

810 47. Vennin, C.; Chin, V.T.; Warren, S.C.; Lucas, M.C.; Herrmann, D.; Magenau, A.;
811 Melenec, P.; Walters, S.N.; del Monte-Nieto, G.; Conway, J.R.W.; et al. Transient
812 Tissue Priming via ROCK Inhibition Uncouples Pancreatic Cancer Progression,
813 Sensitivity to Chemotherapy, and Metastasis. *Sci. Transl. Med.* **2017**, *9*,
814 eaai8504, doi:10.1126/scitranslmed.aai8504.

815 48. Rath, N.; Olson, M.F. Rho-Associated Kinases in Tumorigenesis: Re-Considering
816 ROCK Inhibition for Cancer Therapy. *EMBO Rep* **2012**, *13*, 900–908,
817 doi:10.1038/embor.2012.127.

818 49. Subramanian, A.; Tamayo, P.; Mootha, V.K.; Mukherjee, S.; Ebert, B.L.; Gillette,
819 M.A.; Paulovich, A.; Pomeroy, S.L.; Golub, T.R.; Lander, E.S.; et al. Gene Set
820 Enrichment Analysis: A Knowledge-Based Approach for Interpreting Genome-
821 Wide Expression Profiles. *Proc Natl Acad Sci U S A* **2005**, *102*, 15545–15550,
822 doi:10.1073/pnas.0506580102.

823 50. Kim, D.; Pertea, G.; Trapnell, C.; Pimentel, H.; Kelley, R.; Salzberg, S.L. TopHat2:
824 Accurate Alignment of Transcriptomes in the Presence of Insertions, Deletions
825 and Gene Fusions. *Genome Biol* **2013**, *14*, R36, doi:10.1186/gb-2013-14-4-r36.

826 51. Love, M.I.; Huber, W.; Anders, S. Moderated Estimation of Fold Change and
827 Dispersion for RNA-Seq Data with DESeq2. *Genome Biol* **2014**, *15*, 550,
828 doi:10.1186/s13059-014-0550-8.

829

830 **Figure legends**

831 **Figure 1. Altered apoptotic morphologies of ROCK1nc hepatocytes.**

832 **A.** Primary hepatocytes isolated from ROCK1wt (left panels) or ROCK1nc (right panels)
833 mice were treated with 1 μM ABT-199 to induce apoptosis, then images were capture
834 every 3 minutes by bright field microscopy. Representative images shown at indicated
835 time points. **B.** Scanning electron micrographs of representative ROCK1wt (left) and
836 ROCK1nc (right) hepatocytes. Scale bars = 10 μm.

837

838 **Figure 2. Steatosis and cytokine/chemokine induction by acute DEN treatment of**
839 **primary hepatocytes.**

840 **A.** Haematoxylin and eosin (H&E) staining of representative liver sections from ROCK1wt
841 or ROCK1nc mice 72 hours after DEN injection. Scale bar = 100 μm. **B.** Venn diagram of
842 the number of genes significantly (adjusted $p < 0.05$) changed in expression by at least
843 1.5 fold in ROCK1wt and ROCK1nc livers 72 hours after DEN injection. **C.** Reactome
844 gene sets significantly associated (nominal $p < 0.05$) with genes that were significantly
845 (adjusted $p < 0.05$) altered in expression by at least 1.5 fold in ROCK1wt or ROCK1nc
846 livers 72 hours after DEN injection. **D.** Relative induction of cytokines/chemokines 72
847 hours after DEN injection relative to untreated ROCK1wt and ROCK1nc mice. Means ±
848 standard deviation, n = 5 independent determinations. Unpaired Student's t-test, p values
849 less than 0.05 indicated in bold typeface.

850

851 **Figure 2-figure supplement 1. RNA sequencing of untreated and DEN-treated**
852 **ROCK1wt and ROCK1nc livers.**

853 **A.** Log10-log10 scatter plots of mean RNAseq reads for ROCK1wt livers that had been
854 treated for 72 hours with vehicle vs DEN, where $p < 0.05$ and fold-change (FC) differences
855 > ± 1.5X indicated with green dots, $p \geq 0.05$ or FC ≤ ± 1.5X indicated with grey dots. **B.**
856 Log10-log10 scatter plots of mean RNAseq reads for ROCK1nc livers that had been
857 treated for 72 hours with vehicle vs DEN, where $p < 0.05$ and fold-change (FC) differences
858 > ± 1.5X indicated with red dots, $p \geq 0.05$ or FC ≤ ± 1.5X indicated with grey dots. **C.**
859 Scatter plot of RNAseq $\log_2$ FC for 72 hour treatment with vehicle versus DEN from
860 ROCK1wt and ROCK1nc mouse livers. Dotted line shows Deming regression line with
861 calculated slope = 0.8313. **D.** RNAseq Log2 FC for sequence reads increased in DEN
862 versus vehicle treated ROCK1wt and ROCK1nc mice (left) and for sequence reads
863 decreased in DEN versus vehicle treated ROCK1wt and ROCK1nc mice (right).
864 Horizontal line = median. Unpaired Student's t-test, p values less than 0.05 indicated in
865 bold typeface.

866

867 **Figure 3. Greater steatosis and neutrophil numbers in ROCK1nc liver tumours.**

868 **A.** H&E staining of representative liver tumour sections from ROCK1wt or ROCK1nc mice
869 9 months after DEN treatment. Steatosis was determined on H&E-stained sections as a
870 percentage of the total area from 10 random fields per section per mouse, and graded
871 according to the following criteria: grade 0, < 5%; grade 1, 5-25%; grade 2, 26-50%; grade
872 3, 51-75%; grade 4, > 75%. Scale bars = 100 μm. **B.** Representative

873 Immunohistochemical (IHC) images of anti-S100A9 antibody-stained formalin-fixed
874 paraffin embedded (FFPE) liver sections showing neutrophils (brown) in liver tumours (left
875 panels), and corresponding bar graph (right panel). S100A9 positive neutrophils were
876 scored as number per mm^2 in 5 random fields per section per mouse. **C.** Representative
877 IHC images of anti-F4/80 antibody-stained liver sections showing macrophages numbers
878 in liver tumours (left panels), and corresponding bar graph (right panel). F4/80 positive
879 macrophages were scored as number per mm^2 in 5 random fields per section per mouse.
880 Scale bars = 100 μm. Means ± standard deviation, ROCK1wt n = 10 mice, ROCK1nc n =
881 7 mice. Unpaired Student's t-test, p values less than 0.05 indicated in bold typeface.

882

883 **Figure 3-figure supplement 1. Biochemical markers of liver function and health are**
884 **not different between ROCK1wt and ROCK1nc mice with DEN-induced tumours.**
885 Serum levels of: **A.** total bilirubin; **B.** alkaline phosphatase; **C.** aspartate
886 aminotransferase; **D.** alanine transaminase; **E.** total protein; **F.** albumin; **G.** globulins and
887 **H.** ratio of albumin/globulin were not significantly different between ROCK1wt and
888 ROCK1nc mice with DEN-induced tumours. Means ± standard deviation, ROCK1wt n =
889 12 mice, ROCK1nc n = 11 mice. Unpaired Student's t-test.

890

891 **Figure 4. Greater $CD3^+$ and $CD8^+$ T cell numbers in ROCK1nc liver tumours.**

892 **A.** Representative IHC images of anti-CD3 antibody-stained liver sections showing $CD3^+$
893 T cells (brown) in liver tumours (left panels), and corresponding bar graph (right panel).
894 $CD3^+$ positive T cells were scored as number per mm^2 in 5 random fields per section per

895 mouse. **B.** Representative immunofluorescence images of anti-CD8 antibody-stained
896 liver sections showing $CD8^+$ T cells (red) and DAPI stained cells (blue) in ROCK1nc
897 tumours (left panels), and corresponding bar graph (right panel). $CD8^+$ T cells (red) were
898 scored as a percentage of the total 4′,6-diamidino-2-phenylindole (DAPI; upper panel,
899 blue) cell numbers from 5 random fields per section per mouse **C.** Representative IHC
900 images of anti-Foxp3 antibody-stained liver sections showing $Foxp3^+$ Treg cells (brown)
901 in liver tumours (left panels), and corresponding bar graph (right panel). $Foxp3^+$ Treg cells
902 were scored as number per mm^2 in 5 random fields per section per mouse. Scale bars =
903 100 μm. Means ± standard deviation, ROCK1wt n = 10 mice, ROCK1nc n = 7 mice.
904 Unpaired Student's t-test, p values less than 0.05 indicated in bold typeface.

905

906 **Figure 5. Fewer liver tumours in fasudil treated mice without increased immune cell**
907 **recruitment.**

908 **A.** Timeline of DEN + fasudil treatment regimen. **B.** Macroscopic view of representative
909 livers (scale bars = 10 mm) and representative H&E stained tumour sections (scale bars
910 = 500 μm) from vehicle or fasudil treated mice. **C.** Total tumour numbers in ROCK1wt
911 mice treated with vehicle or fasudil. Means ± standard deviation, n = 13 mice per
912 condition. **D.** Total tumour areas in ROCK1wt mice treated with vehicle or fasudil. Means
913 ± standard deviation, n = 13 mice per condition. **E.** Representative IHC images of anti-
914 S100A9 antibody-stained liver section from fasudil treated mouse showing neutrophils
915 (brown) in liver tumours (left panels), and corresponding bar graph (right panel). S100A9
916 positive neutrophils were scored as number per mm^2 in 5 random fields per section per
917 mouse. Scale bar = 100 μm. Means ± standard deviation, vehicle n = 13 mice, fasudil n

918 = 9 mice. **F.** Representative IHC images of anti-CD8 antibody-stained liver section from
919 fasudil treated mouse showing $CD8^+$ T cells (brown) in liver tumours (left panels), and
920 corresponding bar graph (right panel). $CD8^+$ T cells were scored as number per mm^2 in 5
921 random fields per section per mouse. Means ± standard deviation, vehicle n = 12 mice,
922 fasudil n = 11 mice. Unpaired Student's t-test, p values less than 0.05 indicated in bold
923 typeface.

924

925 **Figure 5-figure supplement 1. No differences in body, liver, lung or spleen weights**
926 **between mice treated with vehicle or fasudil.**

927 Weights at experimental endpoint of: **A.** whole mice; **B.** livers; **C.** livers as a percentage
928 of body weight; **D.** lungs; **E.** lungs as a percentage of body weight; **F.** spleens; **G.** spleens
929 as a percentage of body weight. There were no significant differences between mice
930 treated with vehicle or fasudil. Means ± standard deviation, vehicle n = 13 mice, fasudil n
931 = 13 mice. Unpaired Student's t-test.

932

933 **Figure 5-figure supplement 2. Fewer circulating neutrophils and reduced aspartate**
934 **aminotransferase levels in fasudil treated mice relative to vehicle control.**

935 Blood from vehicle or fasudil treated mice was analyzed for: **A.** Haemoglobin levels;
936 numbers of **B.** platelets; **C.** white cells; **D.** lymphocytes; **E.** monocytes; **F.** neutrophils.
937 Serum from vehicle or fasudil treated mice was analyzed for markers of liver function and
938 health: **G.** bilirubin; **H.** alanine transaminase; **I.** albumin; **J.** alkaline phosphatase; **K.**
939 aspartate aminotransferase; **L.** globulins. Means ± standard deviation, vehicle n = 9 mice,

940 fasudil n = 9 mice. Unpaired Student's t-test, p values less than 0.05 indicated in bold
941 typeface.

942

943 **Figure 6. Fewer liver tumours in AT13148 treated mice without increased immune**
944 **cell recruitment.**

945 **A.** Timeline of DEN + AT13148 treatment regimen. **B.** Macroscopic view of representative
946 livers (scale bars = 10 mm) and representative H&E stained tumour sections (scale bars
947 = 500 μm) from vehicle or AT13148 treated mice. **C.** Total tumour numbers in ROCK1wt
948 mice treated with vehicle or AT13148. Means ± standard deviation, vehicle n = 8 mice,
949 At13148 n = 9 mice. **D.** Total tumour areas in ROCK1wt mice treated with vehicle or
950 AT13148. Means ± standard deviation, vehicle n = 8 mice, At13148 n = 9 mice. **E.**
951 Representative IHC images of anti-S100A9 antibody-stained liver section from AT13148
952 treated mouse showing neutrophils (brown) in liver tumours (left panels), and
953 corresponding bar graph (right panel). S100A9 positive neutrophils were scored as
954 number per mm^2 in 5 random fields per section per mouse. Scale bar = 100 μm. Means
955 ± standard deviation, vehicle n = 5 mice, AT13148 n = 6 mice. **F.** Representative IHC
956 images of anti-CD8 antibody-stained liver section from AT13148 treated mouse showing
957 $CD8^+$ T cells (brown) in liver tumours (left panels), and corresponding bar graph (right
958 panel). $CD8^+$ T cells were scored as number per mm^2 in 5 random fields per section per
959 mouse. Means ± standard deviation, vehicle n = 5 mice, AT13148 n = 6 mice. Unpaired
960 Student's t-test, p values less than 0.05 indicated in bold typeface.

961

962 **Figure 6-figure supplement 1. No differences in body, liver or lung weights between**
963 **mice treated with vehicle or AT13148.**

964 Weights at experimental endpoint of: **A.** whole mice; **B.** livers; **C.** livers as a percentage
965 of body weight; **D.** lungs; **E.** lungs as a percentage of body weight; **F.** spleens; **G.** spleens
966 as a percentage of body weight. There were no significant differences between mice
967 treated with vehicle or AT13148, with the exception of spleen weights that were
968 significantly smaller when comparing weights, but not when compared as percentages of
969 body weights. Means ± standard deviation, vehicle n = 9 mice, AT13148 n = 9 mice.
970 Unpaired Student's t-test.

971

972 **Figure 6-figure supplement 2. No significant differences in circulating blood cells**
973 **or biochemical markers of liver health and function between vehicle or AT13148**
974 **treated mice.**

975 Blood from vehicle or AT13148 treated mice was analyzed for: **A.** haemoglobin levels;
976 numbers of **B.** platelets; **C.** white cells; **D.** lymphocytes; **E.** monocytes; **F.** neutrophils.
977 Serum from vehicle or At13148 treated mice was analyzed for markers of liver function
978 and health: **G.** bilirubin; **H.** alanine transaminase; **I.** albumin; **J.** alkaline phosphatase; **K.**
979 aspartate aminotransferase; **L.** globulins. Means ± standard deviation, vehicle n = 5 mice,
980 AT13148 n = 8 mice. Unpaired Student's t-test, p values less than 0.05 indicated in bold
981 typeface.

982

983 **Figure 7. ROCK inhibitor AT13148 lowered circulating platelet and lymphocyte**
984 **numbers, and reduced immune cell recruitment to livers following acute DEN**
985 **treatment.**

986 ROCK1wt mice were treated with 40 mg/kg AT13148 or vehicle 3 x per week via oral
987 gavage for 10 days, then injected with 100 mg/kg DEN intraperitoneally 3 days prior to
988 sacrifice to induce acute liver damage. Flow cytometry analysis of circulating **A.** platelets
989 and **B.** lymphocytes in vehicle (n = 5) and AT13148 (n = 4) treated mice. Liver cell
990 suspensions were analyzed by flow cytometry to determine the relative proportions of **C.**
991 dendritic cells, **D.** natural killer (NK) cells, **E.** $CD8^+$ T cells and **F.** Kupffer cells from vehicle
992 and AT13148 treated mice (n = 5). Means ± standard deviation. Unpaired Student's t-
993 test, p values less than 0.05 indicated in bold typeface.

994

995 **Figure 7-figure supplement 1. No significant differences in body or liver weights,**
996 **blood haemoglobin levels, or circulating white cells, monocytes or neutrophils**
997 **between vehicle or AT13148 treated mice following acute DEN treatment.**

998 Weights at experimental endpoint of: **A.** whole mice; **B.** livers; **C.** livers as a percentage
999 of body weight. Blood from vehicle or AT13148 treated mice was analyzed for: **D.**
1000 haemoglobin levels; numbers of **E.** white cells; **F.** monocytes; **G.** neutrophils. Means ±
1001 standard deviation, vehicle n = 5 mice, AT13148 n = 4 mice. Unpaired Student's t-test.

1002

1003 **Figure 7-figure supplement 2. Immune cell recruitment to livers following acute**
1004 **DEN treatment in vehicle or AT13148 treated mice.**

1005 Liver cell suspensions were analyzed by flow cytometry to determine the proportions of
1006 immune cells relative to total cell numbers counted of: **A.** recruited macrophages; **B.**
1007 neutrophils; **C.** plasmacytoid dendritic cells; **D.** B cells; **E.** $CD4^+$ T cells; **F.** Tregs; **G.** γδ T
1008 cells; **H.** NKT cells. Means ± standard deviation, vehicle n = 5 mice, AT13148 n = 5 mice.
1009 Unpaired Student's t-test.

1010

1011 **Video 1. Time lapse of apoptotic ROCKwt hepatocytes.**
1012 ROCK1wt hepatocytes were plated on 6-well glass bottom dishes that had been coated
1013 with collagen. Cells were serum-starved overnight prior to induction of apoptosis with 1
1014 μM ABT-199 diluted in serum-free starvation medium. Immediately after induction of
1015 apoptosis, the dishes were transferred to the microscope and brightfield time-lapse
1016 microscopy images were acquired at 3 minute intervals for up to 120 minutes with a 10X
1017 DIC objective using a Nikon TE 2000 microscope with a heated stage and 5% CO_2 gas
1018 line.

1019

1020 **Video 2. Time lapse of apoptotic ROCKnc hepatocytes.**
1021 ROCK1nc hepatocytes were plated on 6-well glass bottom dishes that had been coated
1022 with collagen. Cells were serum-starved overnight prior to induction of apoptosis with 1
1023 μM ABT-199 diluted in serum-free starvation medium. Immediately after induction of
1024 apoptosis, the dishes were transferred to the microscope and brightfield time-lapse
1025 microscopy images were acquired at 3 minute intervals for up to 120 minutes with a 10X
1026 DIC objective using a Nikon TE 2000 microscope with a heated stage and 5% CO_2 gas
1027 line.

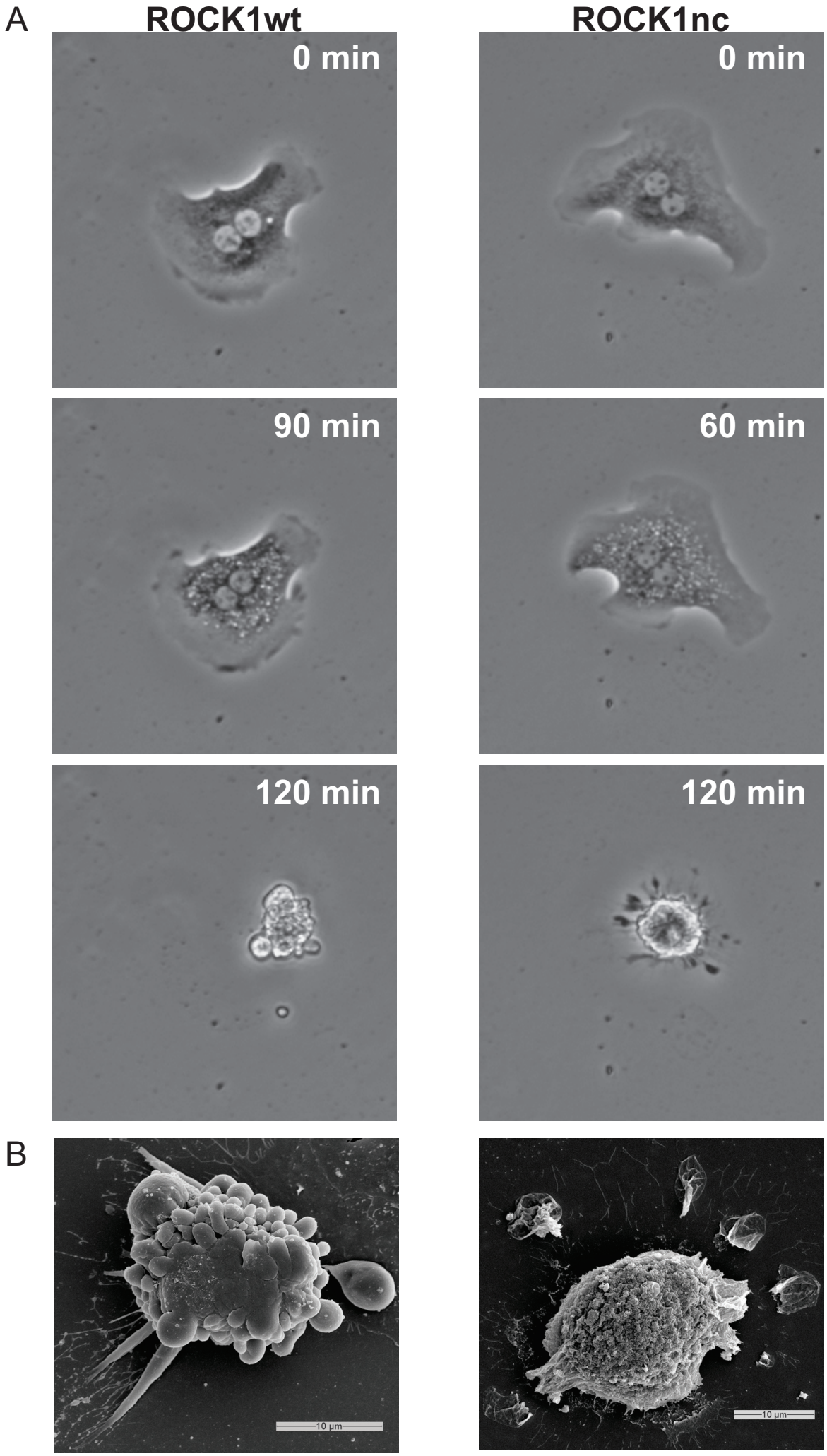
A
ROCK1wt
ROCK1nc
0 min
0 min
90 min
60 min
120 min
120 min
B
10 µm
10 µm

Figure 1

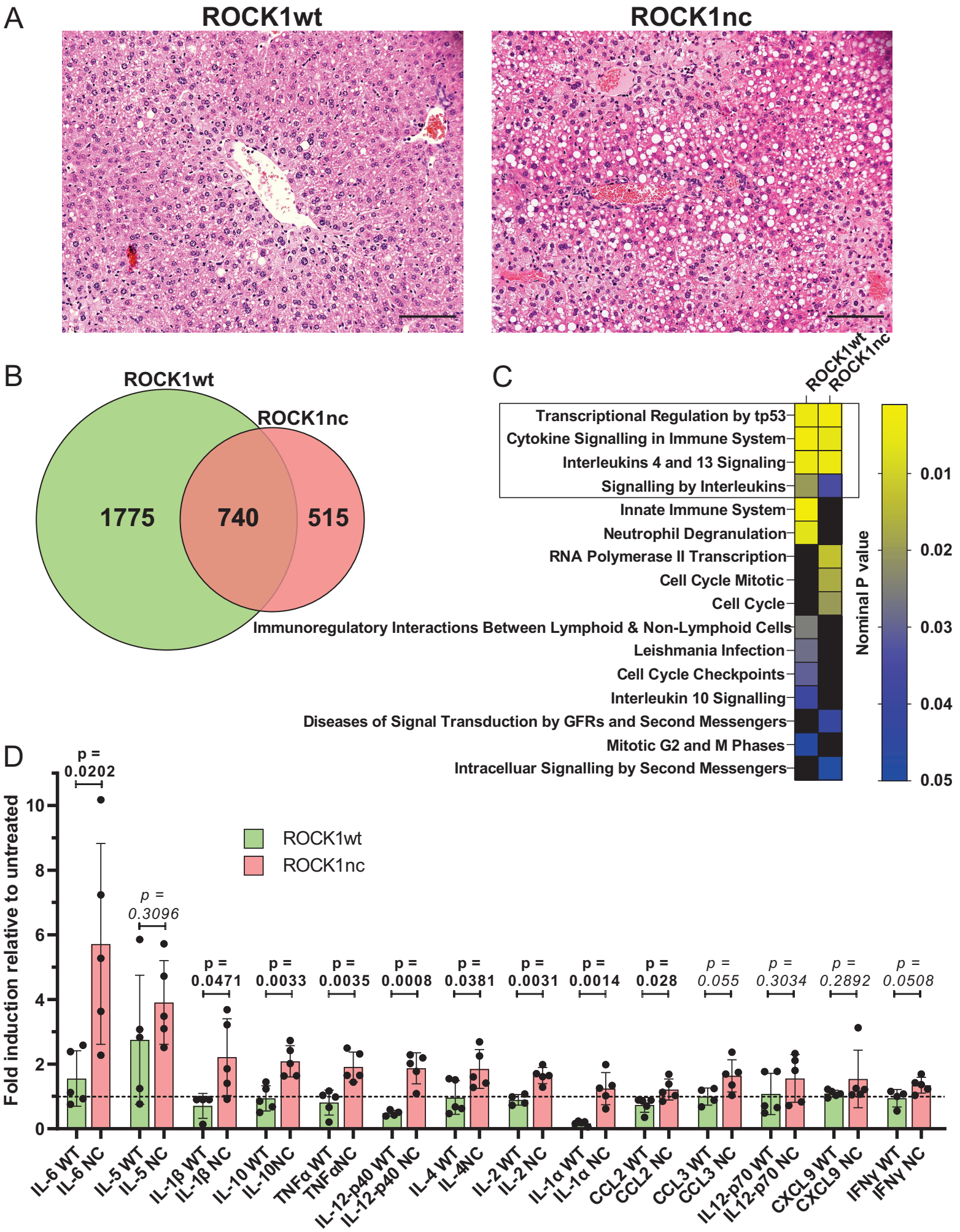
A
ROCK1wt
ROCK1nc
B
ROCK1wt
ROCK1nc
1775
740
515
C
ROCK1wt
ROCK1nc
Transcriptional Regulation by tp53
Cytokine Signalling in Immune System
Interleukins 4 and 13 Signaling
Signalling by Interleukins
Innate Immune System
Neutrophil Degranulation
RNA Polymerase II Transcription
Cell Cycle Mitotic
Cell Cycle
Immunoregulatory Interactions Between Lymphoid & Non-Lymphoid Cells
Leishmania Infection
Cell Cycle Checkpoints
Interleukin 10 Signalling
Diseases of Signal Transduction by GFRs and Second Messengers
Mitotic G2 and M Phases
Intracelluar Signalling by Second Messengers
Nominal P value
0.01
0.02
0.03
0.04
0.05
D
Fold induction relative to untreated
ROCK1wt
ROCK1nc
p = 0.0202
p = 0.3096
p = 0.0471
p = 0.0033
p = 0.0035
p = 0.0008
p = 0.0381
p = 0.0031
p = 0.0014
p = 0.028
p = 0.055
p = 0.3034
p = 0.2892
p = 0.0508
IL-6 WT
IL-6 NC
IL-5 WT
IL-5 NC
IL-1β WT
IL-1β NC
IL-10 WT
IL-10NC
TNFα WT
TNFαNC
IL-12-p40 WT
IL-12-p40 NC
IL-4 WT
IL-4NC
IL-2 WT
IL-2 NC
IL-1α WT
IL-1α NC
CCL2 WT
CCL2 NC
CCL3 WT
CCL3 NC
IL12-p70 WT
IL12-p70 NC
CXCL9 WT
CXCL9 NC
IFNγ WT
IFNγ NC

Figure 2

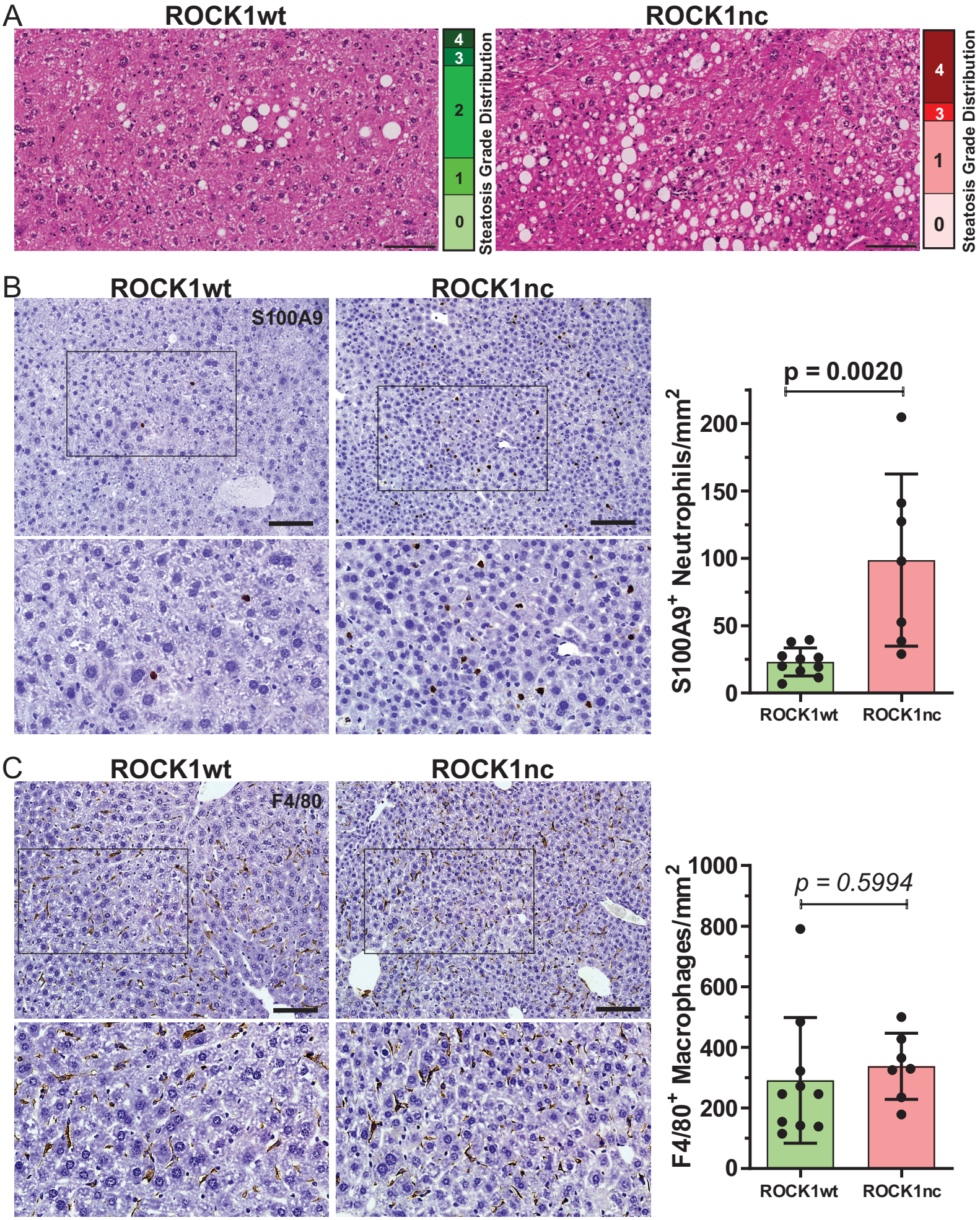
A
ROCK1wt
ROCK1nc
4
3
2
1
0
Steatosis Grade Distribution
B
S100A9
p = 0.0020
S100A9+ Neutrophils/mm2
200
150
100
50
0
ROCK1wt
ROCK1nc
C
F4/80
p = 0.5994
F4/80+ Macrophages/mm2
1000
800
600
400
200
0

Figure 3

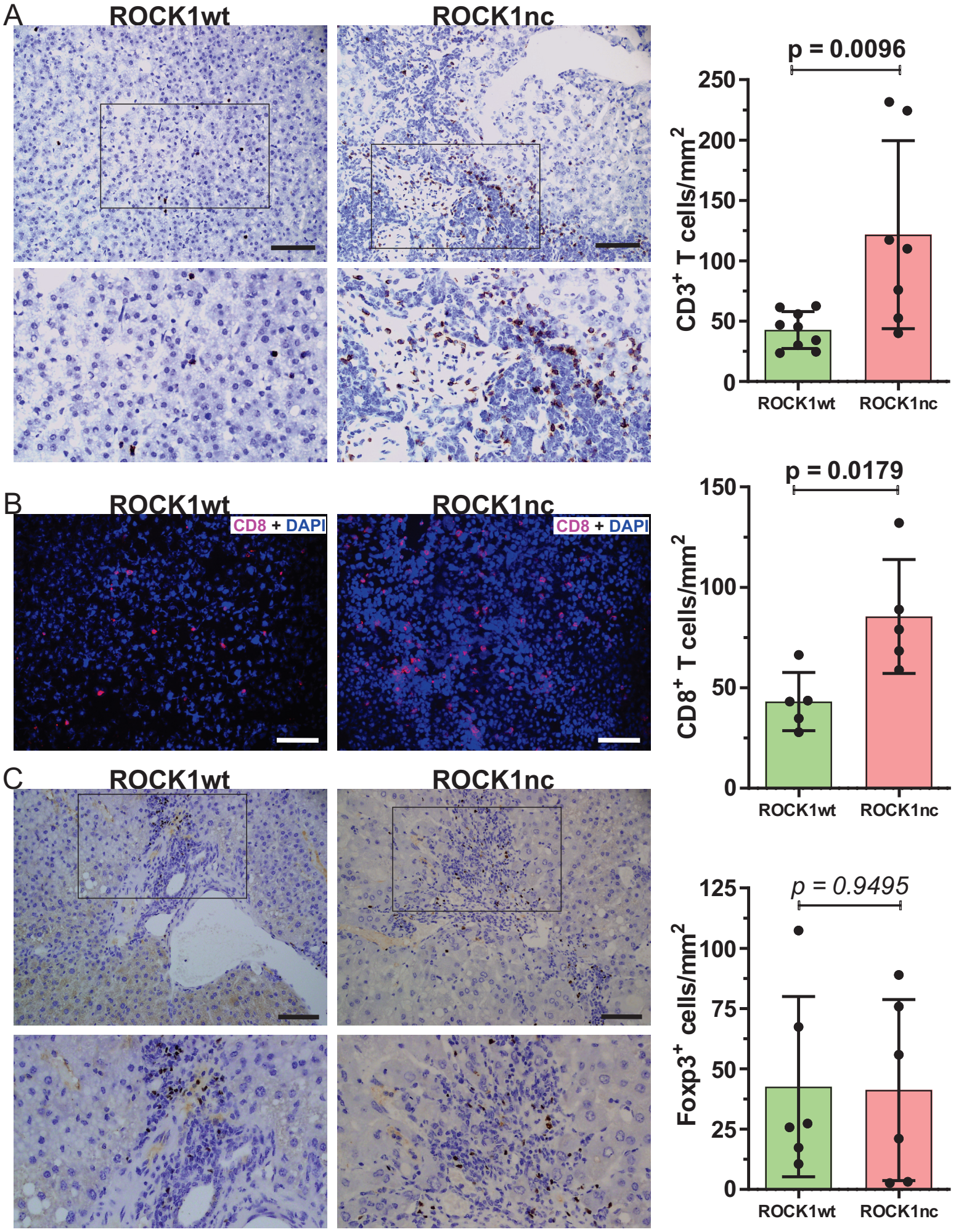
A
ROCK1wt
ROCK1nc
p = 0.0096
CD3+ T cells/mm2
250
200
150
100
50
0
ROCK1wt
ROCK1nc
B
ROCK1wt
ROCK1nc
CD8 + DAPI
CD8 + DAPI
p = 0.0179
CD8+ T cells/mm2
150
100
50
0
ROCK1wt
ROCK1nc
C
ROCK1wt
ROCK1nc
p = 0.9495
Foxp3+ cells/mm2
125
100
75
50
25
0
ROCK1wt
ROCK1nc

Figure 4

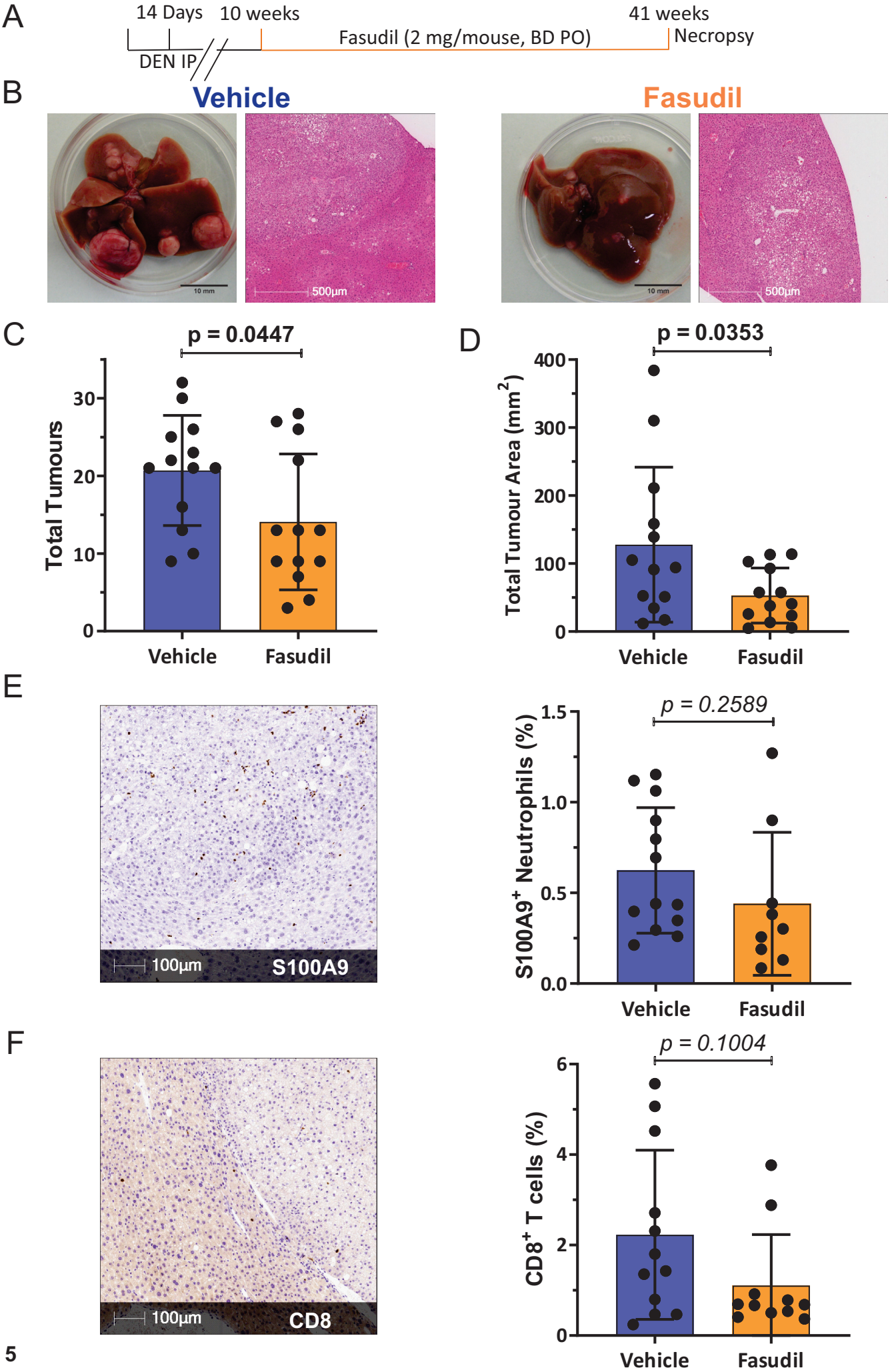
A
14 Days
10 weeks
41 weeks
DEN IP
Fasudil (2 mg/mouse, BD PO)
Necropsy
B
Vehicle
Fasudil
10 mm
500µm
C
p = 0.0447
Total Tumours
Vehicle
Fasudil
D
p = 0.0353
Total Tumour Area (mm²)
E
100µm
S100A9
p = 0.2589
S100A9⁺ Neutrophils (%)
F
CD8
p = 0.1004
CD8⁺ T cells (%)

Figure 5

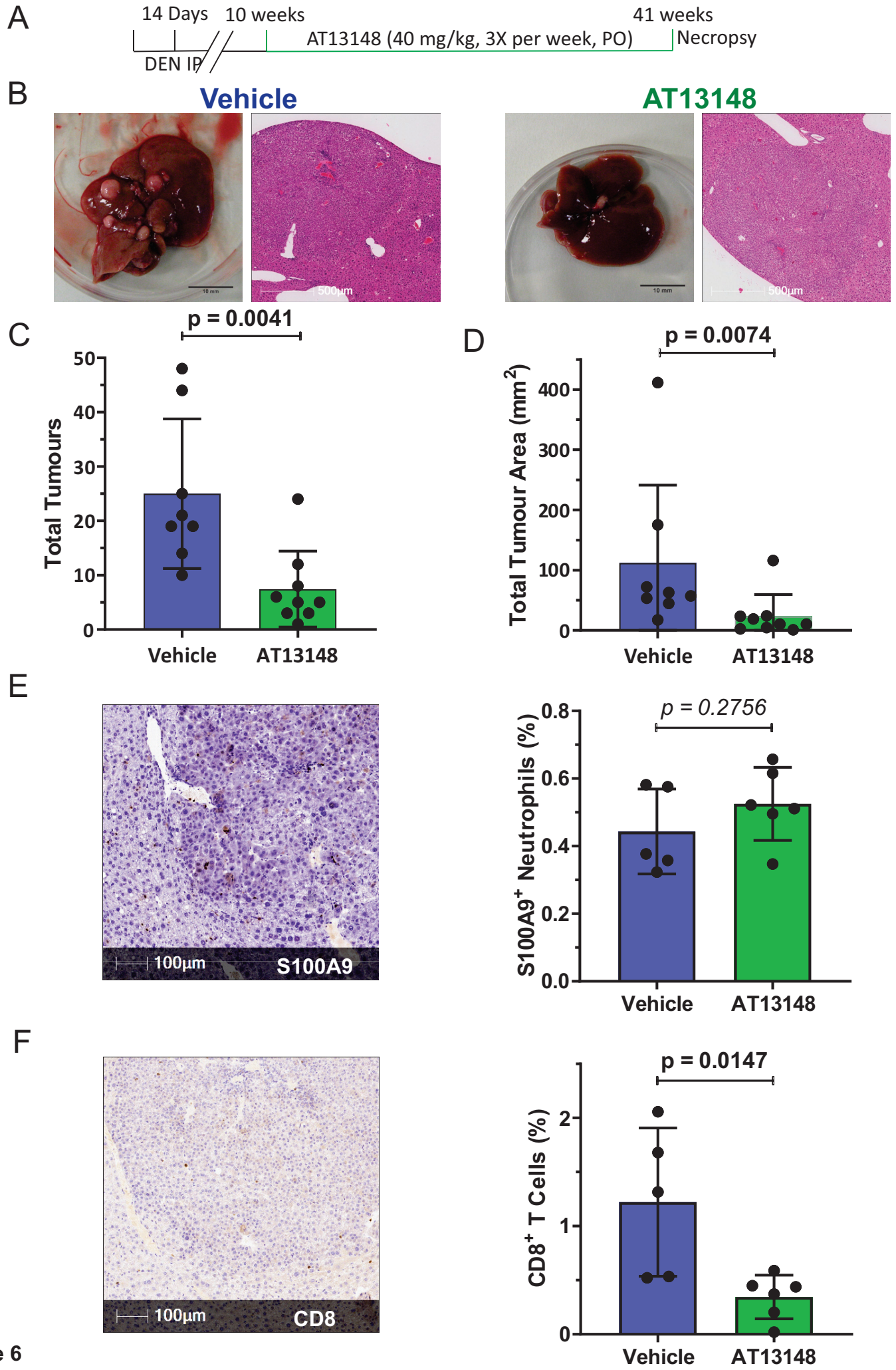
A
14 Days
10 weeks
41 weeks
DEN IP
AT13148 (40 mg/kg, 3X per week, PO)
Necropsy
B
Vehicle
AT13148
C
p = 0.0041
Total Tumours
Vehicle
AT13148
D
p = 0.0074
Total Tumour Area (mm2)
Vehicle
AT13148
E
100µm
S100A9
p = 0.2756
S100A9+ Neutrophils (%)
Vehicle
AT13148
F
100µm
CD8
p = 0.0147
CD8+ T Cells (%)
Vehicle
AT13148

Figure 6

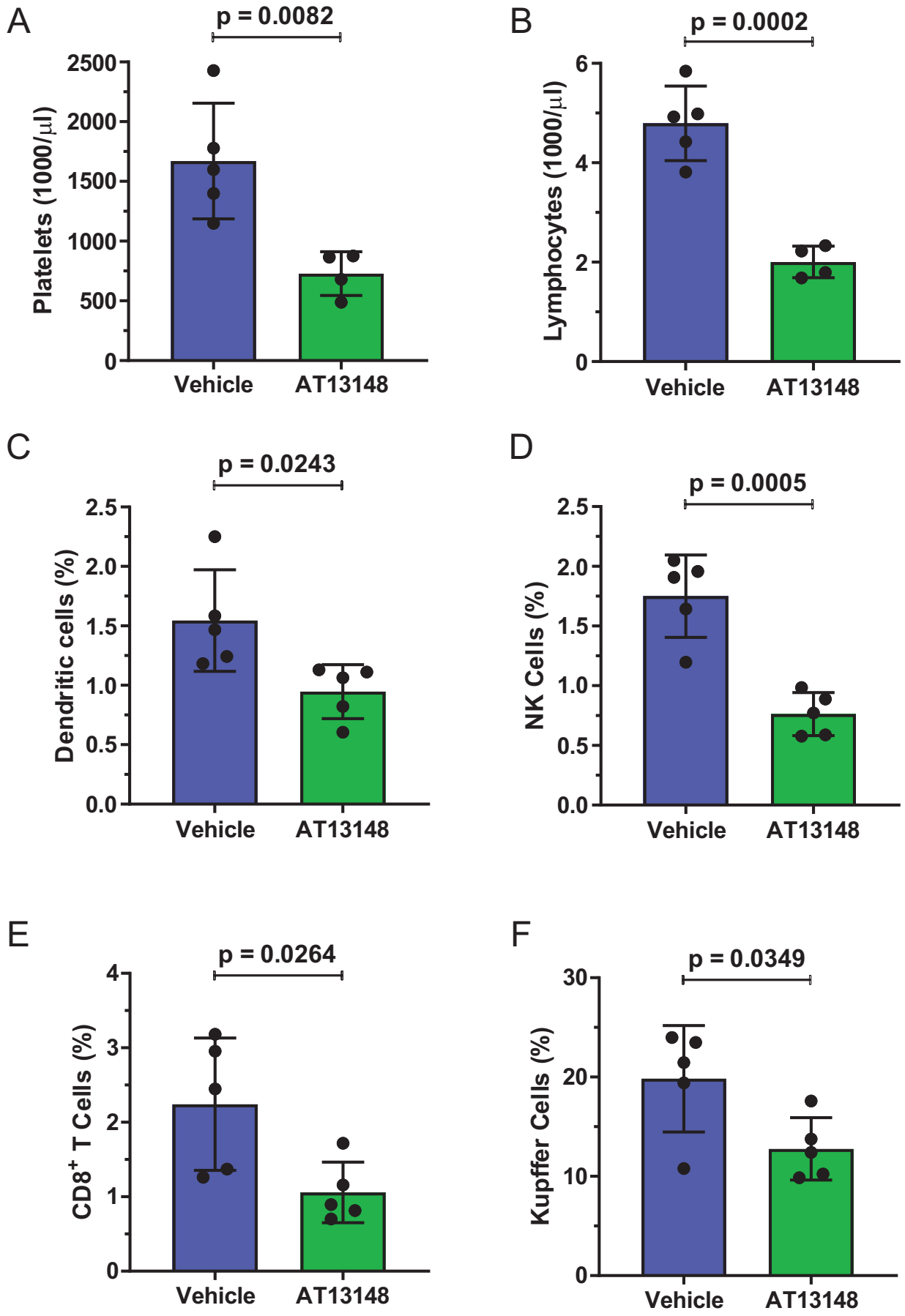
A
p = 0.0082
Platelets (1000/μl)
2500
2000
1500
1000
500
0
Vehicle
AT13148
B
p = 0.0002
Lymphocytes (1000/μl)
6
4
2
0
Vehicle
AT13148
C
p = 0.0243
Dendritic cells (%)
2.5
2.0
1.5
1.0
0.5
0.0
Vehicle
AT13148
D
p = 0.0005
NK Cells (%)
2.5
2.0
1.5
1.0
0.5
0.0
Vehicle
AT13148
E
p = 0.0264
CD8+ T Cells (%)
4
3
2
1
0
Vehicle
AT13148
F
p = 0.0349
Kupffer Cells (%)
30
20
10
0
Vehicle
AT13148

Figure 7

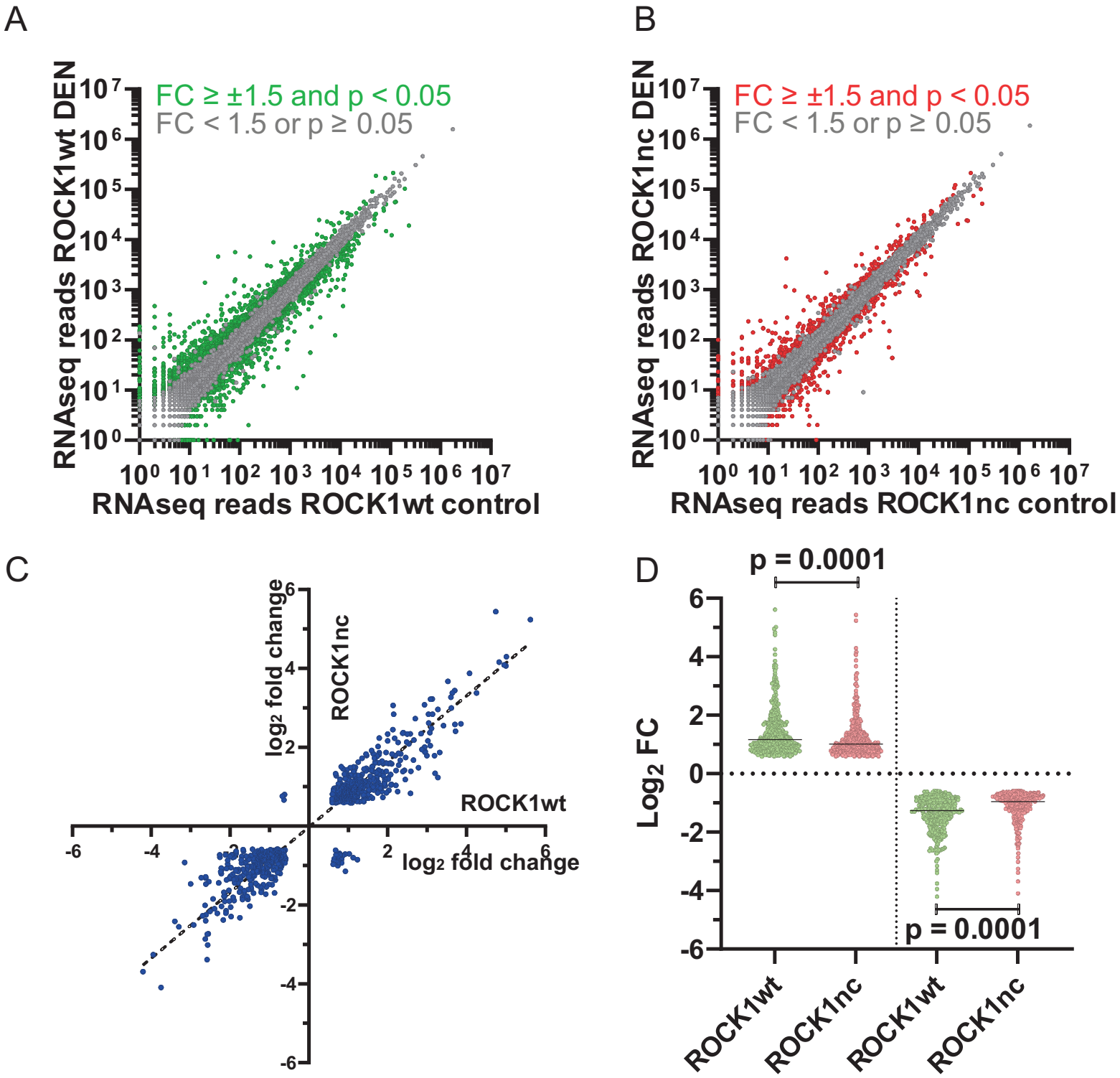

Figure 2-figure supplement 1

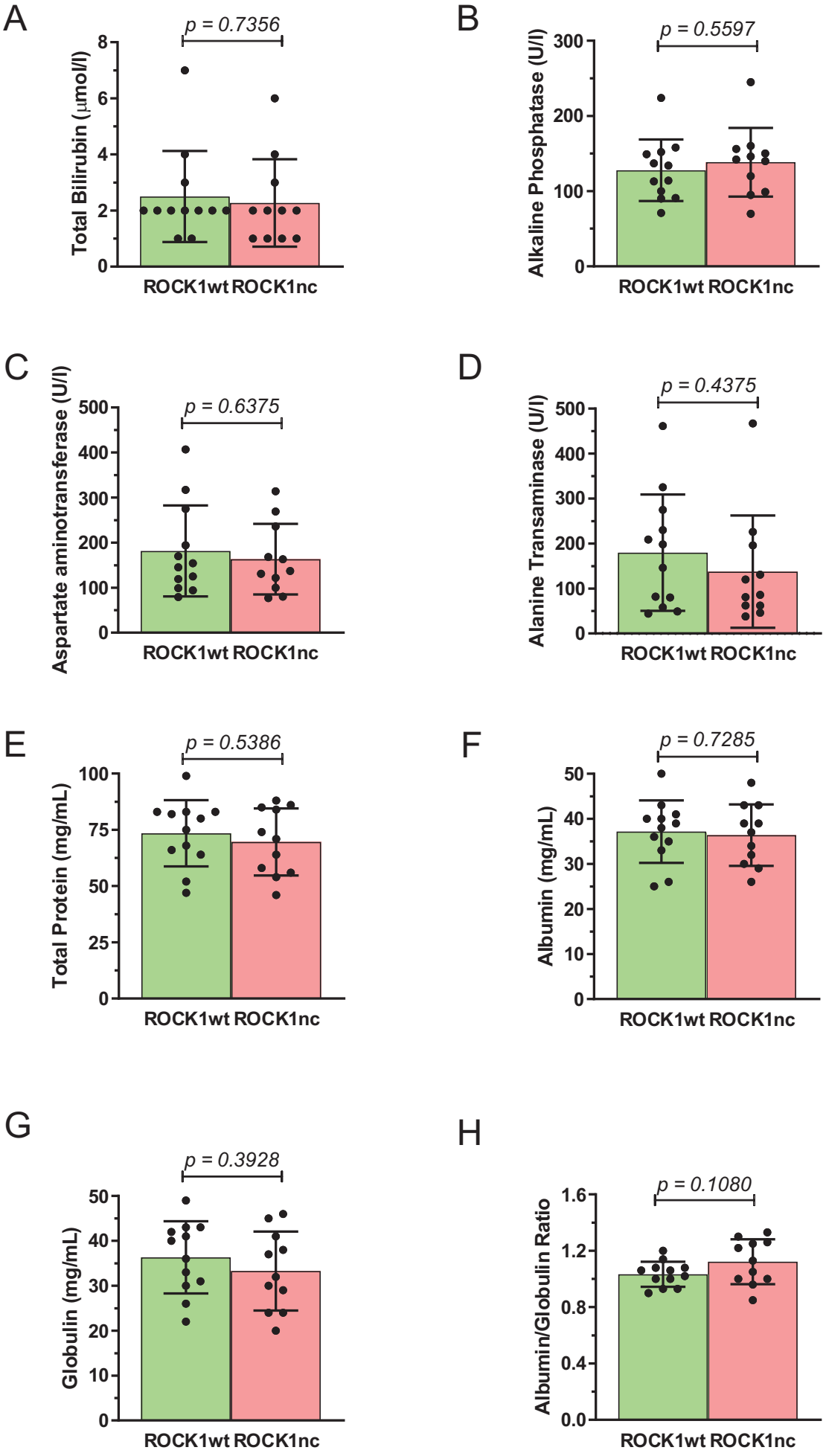

Figure 3-figure supplement 1

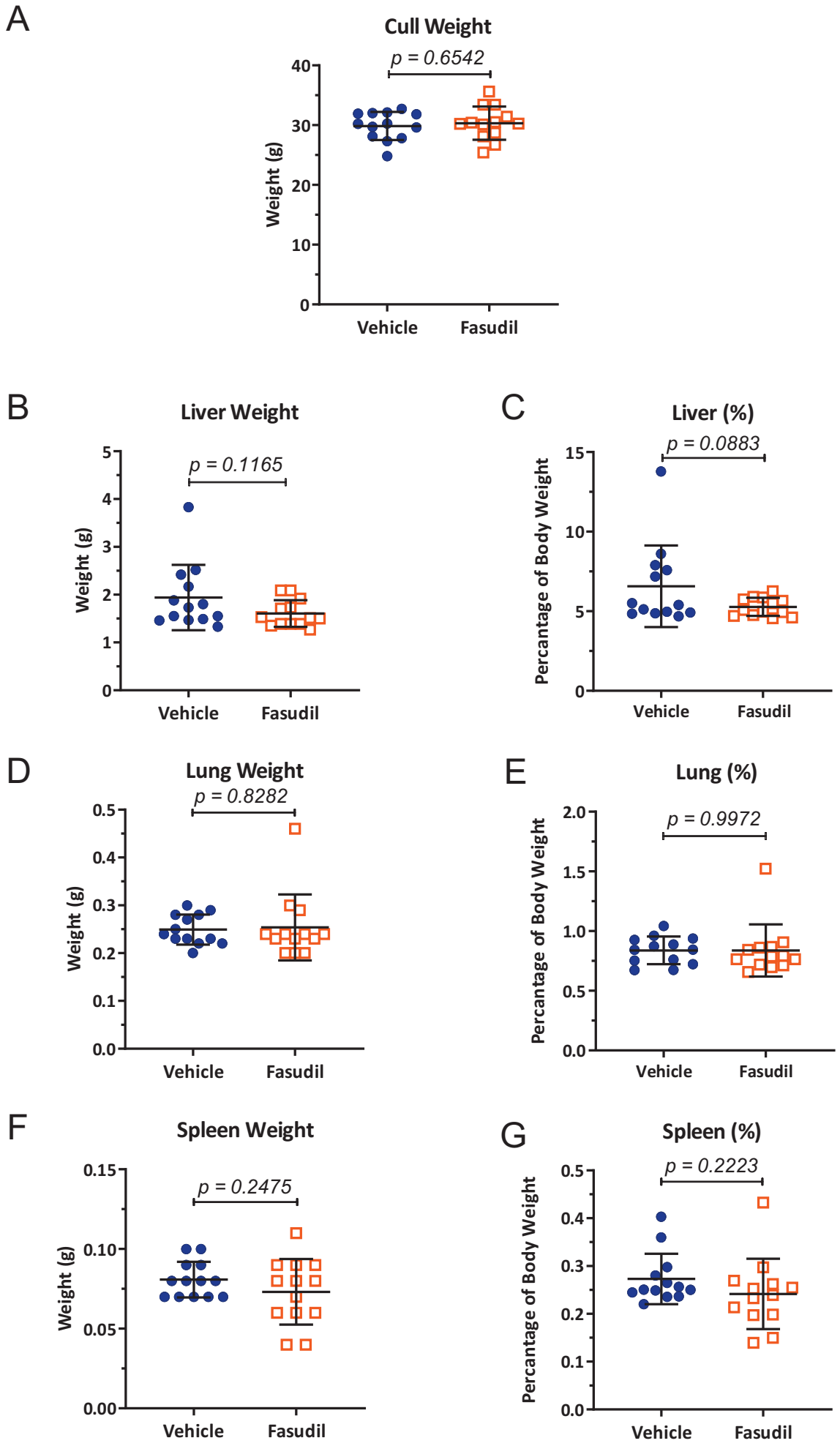

Figure 5-figure supplement 1

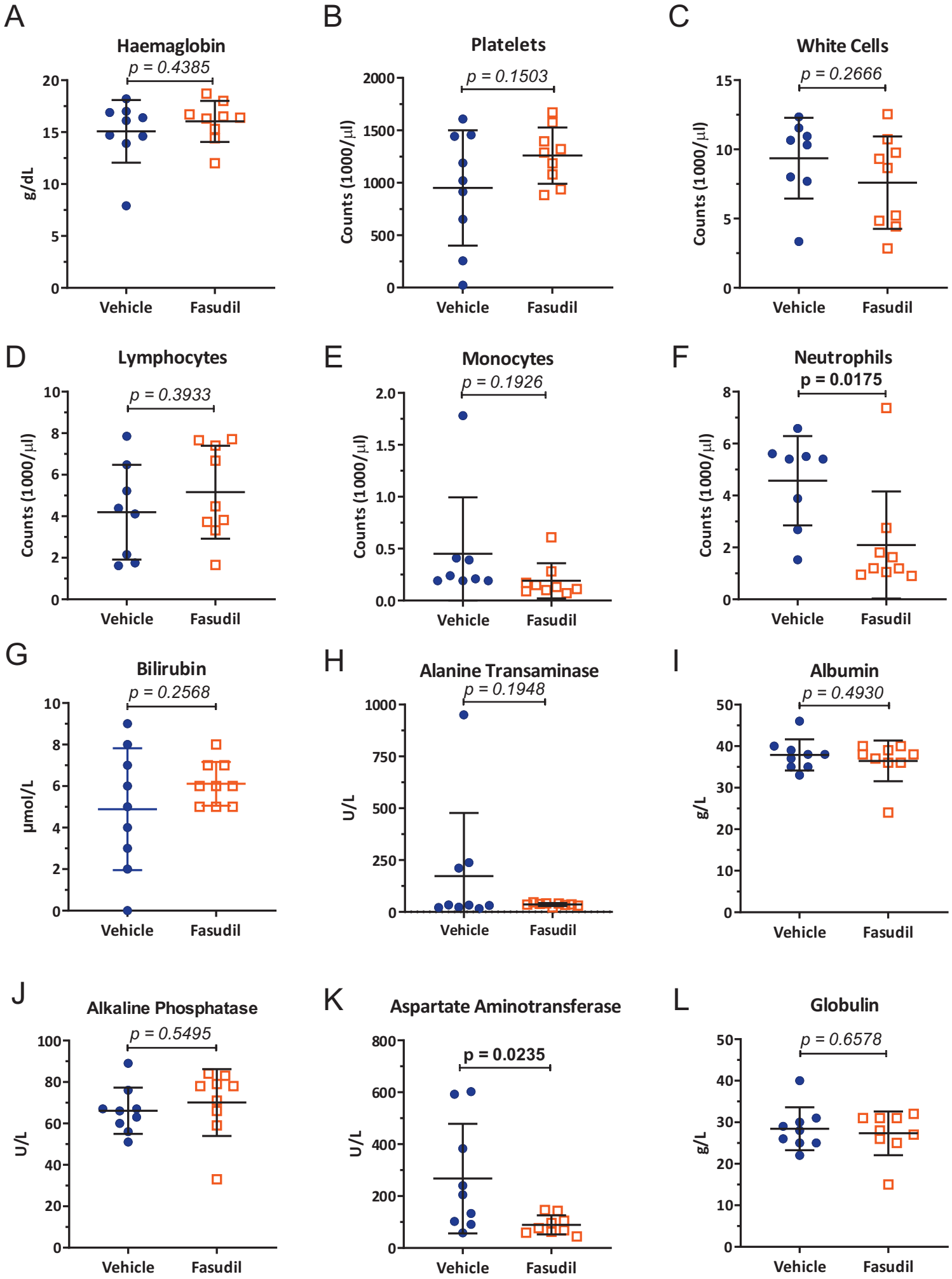

Figure 5-figure supplement 2

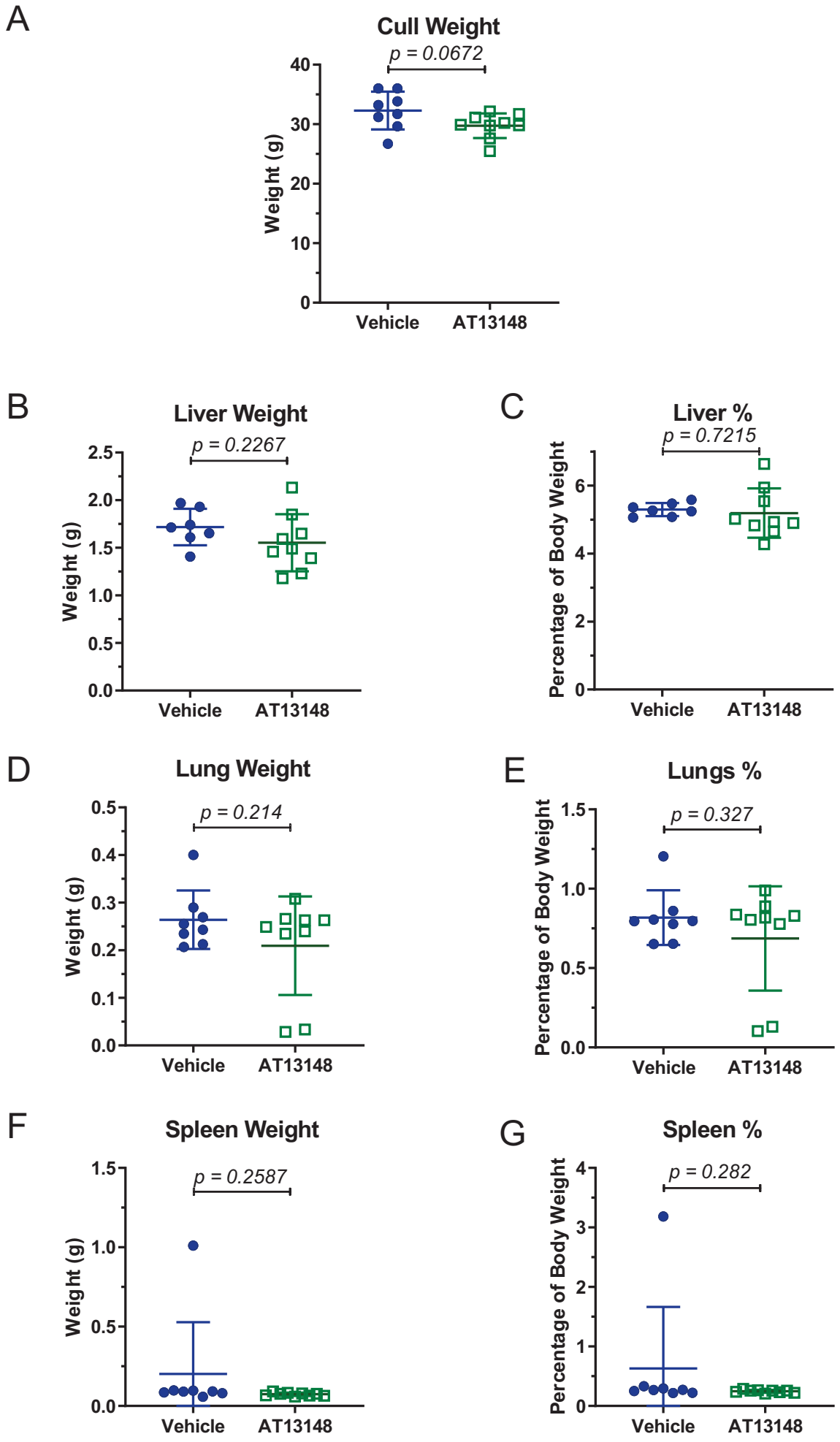

Figure 6-figure supplement 1

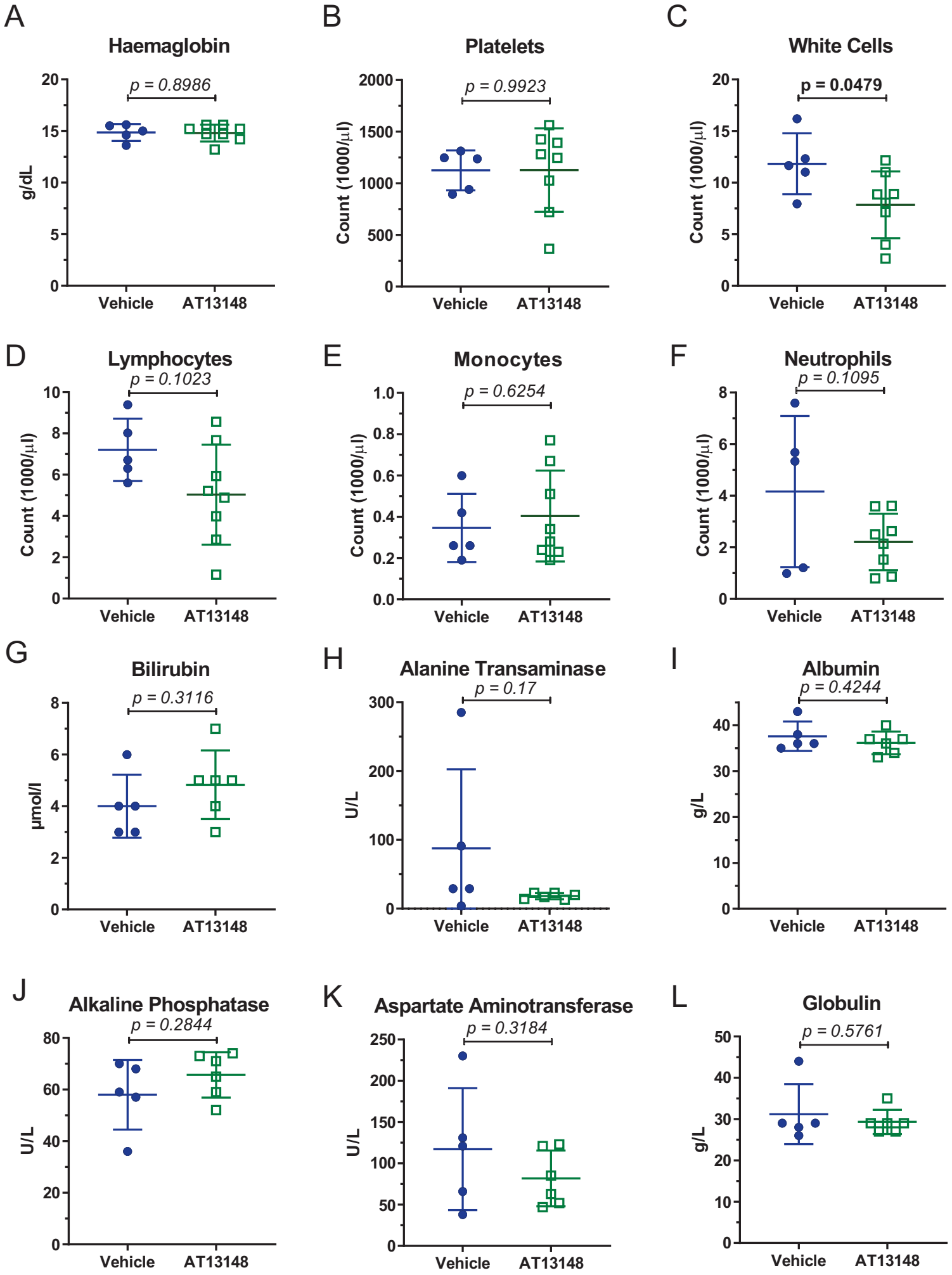

Figure 6-figure supplement 2

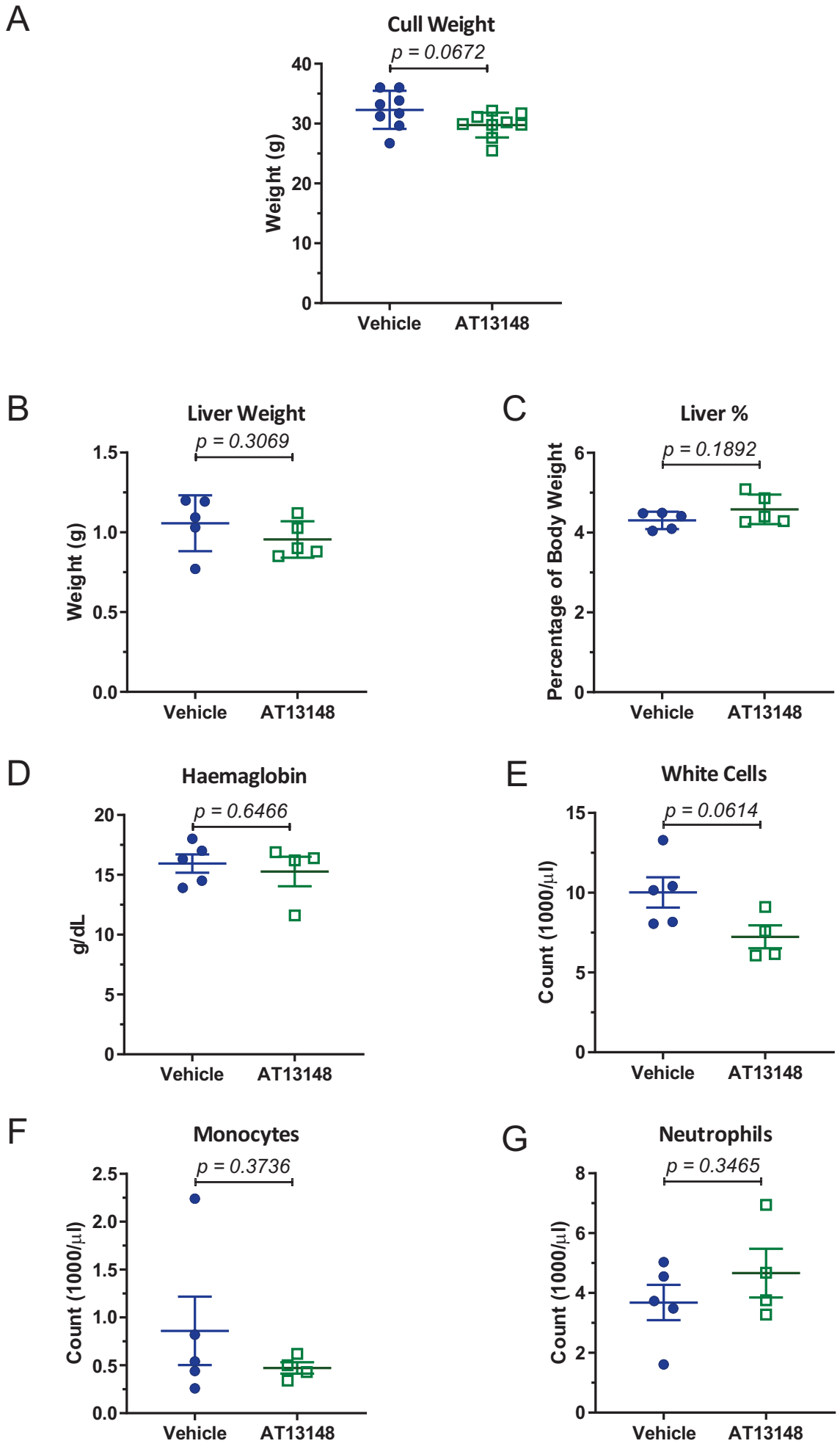

Figure 7-figure supplement 1

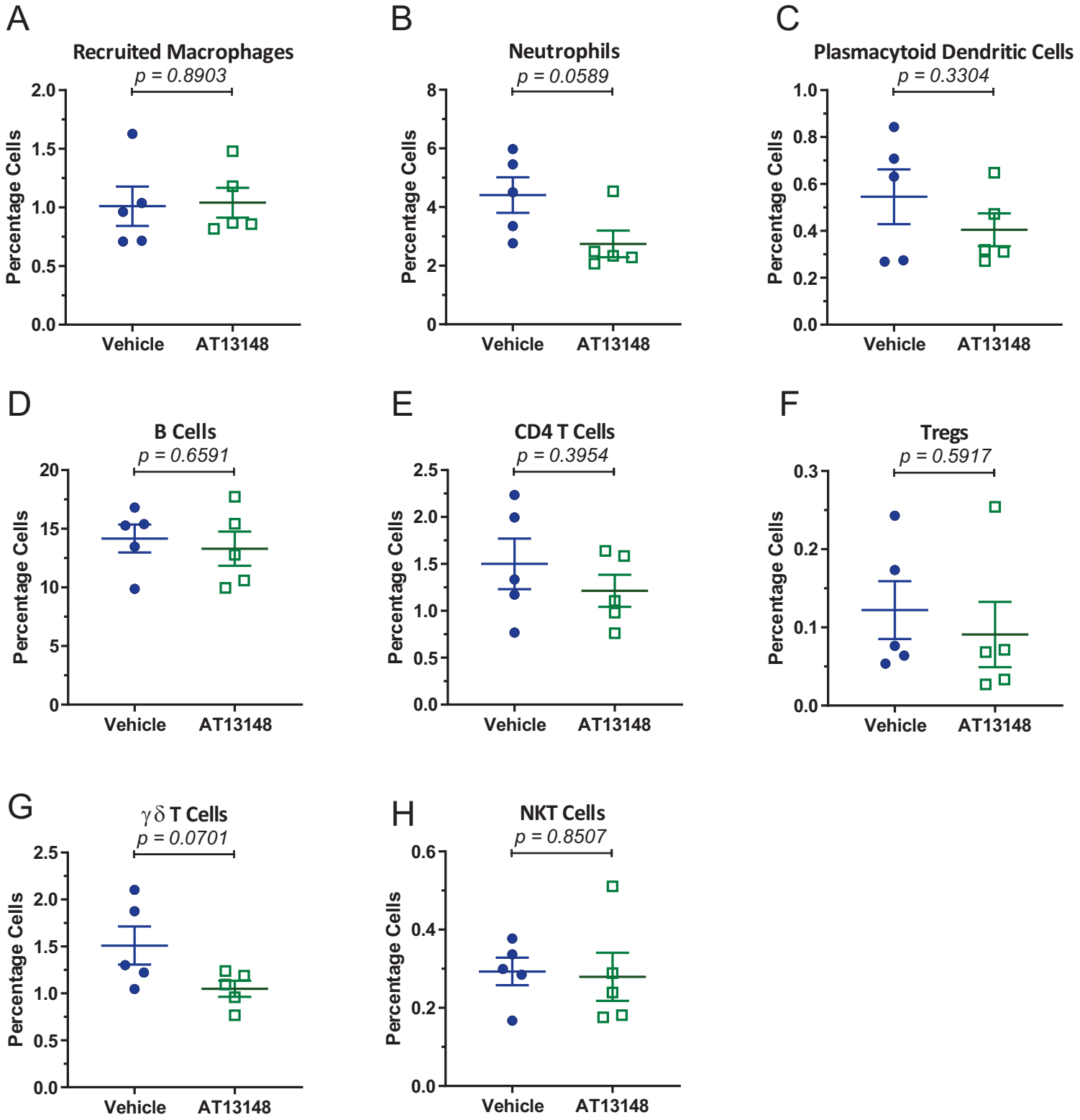

Figure S7-figure supplement 2